

Meet-in-the-Middle Attack on Primitives with Binary Matrix Linear Layer

Qingliang Hou¹, Kuntong Li¹, Guoyan Zhang^{1,2(✉)}, Yanzhao Shen²,
Qidi You^{3,4}, and Xiaoyang Dong⁵

¹ School of Cyber Science and Technology, Shandong University, Qingdao, China
{qinglianghou, likuntong}@mail.sdu.edu.cn, guoyanzhang@sdu.edu.cn

² Shandong Institute of Blockchain, Jinan, China
shenyanzhao@sdibc.cn

³ State Key Laboratory of Space-Ground Integrated Information Technology
youqd@spacestar.com.cn

⁴ Space star Technology Co., Ltd

⁵ Institute for Advanced Study, BNRist, Tsinghua University, Beijing, China
xiaoyangdong@tsinghua.edu.cn

Abstract. Meet-in-the-middle (MitM) is a powerful approach for the cryptanalysis of symmetric primitives. In recent years, MitM has led to many improved records about key recovery, preimage and collision attacks with the help of automated tools. However, most of the previous work target AES-like hashing where the linear layer is an MDS matrix. And we observe that their automatic model for MDS matrix is not suitable for primitives using a binary matrix as their linear layer. In this paper, we propose the **n-XOR** model to describe the XOR operation with an arbitrary number of inputs. And it can be applied to primitives with a binary matrix of arbitrary size. Then, we propose a check model to eliminate the possible inaccuracies caused by **n-XOR**. But the check model is limited by the input size (not greater than 4). Combined with the two new models, we find a MitM key recovery attack on 11-round **Midori64**. When the whitening keys are excluded, a MitM key recovery attack can be mounted on the 12-round **Midori64**. Compared with the previous best work, both of the above results have distinct advantages in terms of reducing memory and data complexity. At last, we apply the **n-XOR** model to the hashing modes of primitives with large size binary matrix. The preimage attack on weakened **Camellia-MMO** (without FL/FL^{-1} and whitening layers) and **Aria-DM** are both improved by 1 round.

Keywords: Meet-in-the-Middle · Binary Matrix · Key Recovery · Preimage · **Midori64** · **Camellia** · **Aria**.

1 Introduction

The Meet-in-the-middle (MitM) is a powerful cryptanalysis strategy first proposed by Diffie and Hellman to attack Double DES [12]. The core idea is to

First Author and Second Author contributed equally to this work.

40 identify two disjoint neutral sets of unknown values. Then, the whole compu-
 41 tation path can be divided into two independent chunks, which are determined
 42 by two neutral sets and denoted by *forward chunk* and *backward chunk*, respec-
 43 tively. At last, the two chunks will meet at a common internal state where the
 44 consistency is checked to filter out candidate assignments of unknown values.
 45 From then on, MitM and its variants have been successfully applied to many
 46 block ciphers [9,32,18,29]. At SAC 2008, Aumasson *et al.* [3] first introduced the
 47 theory of MitM into preimage attacks on step-reduced MD5 and 3-pass HAVAL.
 48 Sequentially, many refined techniques were proposed to enhance the power of
 49 MitM, such as splice-and-cut [2], initial structure [30], bicliques [8], and so on.
 50 At FSE 2011, Sasaki [26] applied such MitM preimage attack to the PGV [25]
 51 hashing modes of AES and presented the first preimage attack on 7-round AES-
 52 MMO/MP/DM together with the partial indirect matching technique. Interestingly,
 53 these enhancements were finally found to be applicable in the key recovery at-
 54 tack on block ciphers. At ACISP 2011, Wei *et al.* [37] broke the full round
 55 KTANTAN using the splice-and-cut technique by connecting the plaintext and
 56 ciphertext with encryption or decryption oracles with only 4 chosen plaintexts.

57 Despite being clear that a MitM attack is entirely determined by its *char-*
 58 *acteristic*, i.e., the configuration for two chunks, it's still complicated and error-
 59 prone to explore the whole configuration space. Recently, automated tools were
 60 introduced to find the best characteristic by solving an optimization problem. At
 61 Eurocrypt 2021, Bao *et al.* [6] proposed an MILP-based MitM preimage attack
 62 on AES-like hash and Haraka v2. At CRYPTO 2021, Dong *et al.* [13] extended
 63 the automatic model into key-recovery and collision attacks and introduced a
 64 table-based method to solve the non-linear constraints imposed on neutral sets.
 65 At CRYPTO 2022, Bao *et al.* [7] considered the MitM attack in a view of su-
 66 perposition (SupP) states and bi-directional attribute propagation (BiDir) such
 67 that neutral sets are treated independently and can be imposed constraints in
 68 both computation paths. At Asiacrypt 2023, Hou *et al.* [17] introduced the SupP
 69 framework into Feistel-based hash functions. At Eurocrypt 2024, Chen *et al.* [10]
 70 considered the linearization of the S-Box in AES and allowed a linear combina-
 71 tion of two neutral sets in the initial structure. Different from the above work,
 72 Schrottenloher and Stevens [33] studied a simple top-down modeling paradigm
 73 for both classical and quantum preimage attacks against permutations and was
 74 later extended to key recovery attack on block ciphers with simple key sched-
 75 ules [34]. The simplified attack excluded many details. In this paper, we adopt
 76 the bottom-up MitM framework in [7] and the table-based method in [13].

77 In the previous work, the targets are most built by a block cipher with an
 78 MDS matrix. Through the diffusion layer, each output cell is related to all the
 79 input cells. However, the primitives with binary matrix are rarely studied, where
 80 each output cell is represented as the XOR of partial input cells. In [13], Dong
 81 *et al.* introduced the 3-XOR model for SKINNY- $n-3n$. In their model, the number
 82 of input cells is fixed to be 4. All valid cases can be easily exhausted to form a
 83 system of inequalities using the convex hull method [36]. However, if more input
 84 cells are involved, the number of valid cases will increase extremely leading to

larger size of system of inequalities, which can make model infeasible to compute. Hence, there is a gap to find an accurate and effective method to describe the MitM attribute propagation through a binary matrix of arbitrary size.

Our Contributions. In this paper, we propose a novel model called **n-XOR** under the encoding scheme in [7], to describe the propagation of MitM attributes through an **XOR** operation with an arbitrary number of input cells. And the number of inequalities formed by **n-XOR** is fixed, independent of the number of inputs. Hence, **n-XOR** can be applied to large binary matrices effectively. However, we also observe that only applying **n-XOR** will lead to subtle inaccuracies. An extremely explicit case is that the constraint on the same neutral bits may be double counted in two different **n-XOR** operations. Besides, there are more implicit cases depending on the specific linear layer. Hence, we propose an additional check model to eliminate these inaccuracies. But this model is limited by the input size n , that is, $n \leq 4$ in our paper.

As a proof of work, we first apply the two new models to **Midori64** [5], with a 4×4 binary matrix as linear layer. Then, an 11-round key recovery attack is found with time complexity of 2^{124} . The data and memory complexity are 2^{36} and 2^6 , respectively. When omitting the whitening layer, a 12-round MitM characteristic for weakened **Midori64** is found with time complexity of 2^{120} . The data and memory cost are 2^{48} and $2^{10.6}$, respectively. Besides, the data and memory complexity can be further reduced if the time complexity is relaxed to 2^{124} . Compared to the previous best records of **Midori64** [23,35,22], despite a little higher time complexity, our results have distinct advantages in reducing data and memory complexity.

It's a practical design strategy to build hash functions on widely used block cipher with a longstanding record of cryptanalysis. And **AES-MMO** was even internationally standardized by ISO [19]. Since **Camellia** [1] was also standardized by ISO [20] and **Aria** [21] was standardized by Korean Standard (KS X1213), the hashing modes of **Camellia** or **Aria** may be potential candidates used in practice. Indeed, their security have been evaluated in a series of works [31,27,16,4]. In this paper, we apply the **n-XOR** to describe the MitM attributes propagation through the large binary matrix of **Camellia** and **Aria**. Finally, we find a preimage attack on 14-round weakened **Camellia-MMO** (without FL/FL^{-1} and whitening layers) and a preimage attack on 6-round **Aria-DM**. Compared to the previous best records [28,16], the attack rounds are both improved by 1 round.

Our results are also summarized in Table 1 and Table 2. For the source code, please refer to <https://github.com/wenny-kt/MITM-Binary-Matrix>.

The rest of this paper is organized as follows. In Section 2, we give an overview of how the automated MitM attacks are deployed, along with some enhanced techniques. In Section 3, we introduce two new improved models embedded in the automated MitM framework, called **n-XOR** and check model. The applications to **Midori64**, **Camellia-MMO** and **Aria-DM** are presented in Sects. 4, 5 and 6, respectively. Finally, we conclude in Section 7.

Table 1: Single Key attacks on Midori64, where ID and \mathcal{DS} -MitM denote impossible differential and Demirci-Selçuk MitM attack, respectively.

Target	Rounds	Data	Memory(Bytes)	Time(Enc.)	Technique	Ref.
Midori64	11	2^{60}	$2^{95.8}$	$2^{116.6}$	ID	[23]
	11	2^{53}	$2^{92.2}$	2^{122}	\mathcal{DS} -MitM	[22]
	11	2^{36}	2^6	2^{124}	MitM	Section 4.1
	12	$2^{55.5}$	2^{109}	$2^{125.5}$	\mathcal{DS} -MitM	[22]
	12 [†]	$2^{61.9}$	2^{44}	$2^{90.5}$	ID	[35]
	12 [†]	2^{48}	$2^{10.6}$	2^{120}	MitM	Section 4.2
	12 [†]	2^{36}	$2^{5.6}$	2^{124}	MitM	Section 4.2

† Weakened version without whitening layers.

Table 2: A Summary of the MitM Attacks on Hashing Modes.

Target	Attacks	Rounds	Time1	Time2	Memory	Technique	Ref.
Camellia-MM0	Preimage	13 [‡]	2^{120}	2^{125}	2^8	MitM	[28]
		14 [‡]	2^{120}	2^{125}	2^8	MitM	Section 5
Aria-DM	Preimage	5	2^{120}	2^{125}	2^8	MitM	[16]
		6	2^{120}	2^{125}	2^{112}	MitM	Section 6

‡ Weakened version without FL/FL^{-1} and whitening layers.

- Time1 represents the time complexity of pseudo-preimage. Time2 represents the time complexity of preimage attack converted from the pseudo-preimage attack according to [24, Fact9.99].

2 Preliminaries: Automated Meet-in-the-Middle Attack

In this section, we provide an overview of how the MitM attack framework is constructed, and how it is encoded into the MILP language with specified configurations for the preimage and key recovery attack. Then, we recall two enhanced techniques to improve the power of MitM attack. The first one is the *table-based method* introduced in [13] to solving the non-linear constraints. Another one is the *Superposition (SupP) States and Bi-direction Attribute-Propagation (BiDir)* introduced in [7] to preserving more valid solutions.

2.1 Framework of the Meet-in-the-Middle Attack

The MitM attack framework is illustrated in Figure 1. \mathcal{S}^{ENC} and \mathcal{S}^{KEY} are the starting states where there are $\lambda_{\mathcal{B}}^{\text{ENC}}$ and $\lambda_{\mathcal{B}}^{\text{KEY}}$ neutral bits for forward computation denoted by ■, and there are $\lambda_{\mathcal{R}}^{\text{ENC}}$ and $\lambda_{\mathcal{R}}^{\text{KEY}}$ neutral bits for backward computation denoted by ■. After imposing $l_{\mathcal{R}}^{\text{ENC}}$ and $l_{\mathcal{R}}^{\text{KEY}}$ constraints on $\lambda_{\mathcal{R}}^{\text{ENC}}$ and $\lambda_{\mathcal{R}}^{\text{KEY}}$ backward neutral bits, respectively, ■ can be propagated to the matching points $End_{\mathcal{B}}$ independent of the ■ bits. The degree of freedom (DoF) for the ■ neutral space is computed by $d_{\mathcal{R}} = \lambda_{\mathcal{R}}^{\text{ENC}} + \lambda_{\mathcal{R}}^{\text{KEY}} - l_{\mathcal{R}}^{\text{ENC}} - l_{\mathcal{R}}^{\text{KEY}}$. Similarly, forward neutral bits are imposed on $l_{\mathcal{B}}^{\text{ENC}}$ and $l_{\mathcal{B}}^{\text{KEY}}$ constraints to cancel the effect of ■ in the backward computation. The DoF of the ■ neutral space can be computed by $d_{\mathcal{B}} = \lambda_{\mathcal{B}}^{\text{ENC}} + \lambda_{\mathcal{B}}^{\text{KEY}} - l_{\mathcal{B}}^{\text{ENC}} - l_{\mathcal{B}}^{\text{KEY}}$. Through a feed-forward mechanism or querying a public Encryption-Decryption oracle, $End_{\mathcal{R}}$ can be derived by ■. Instead of

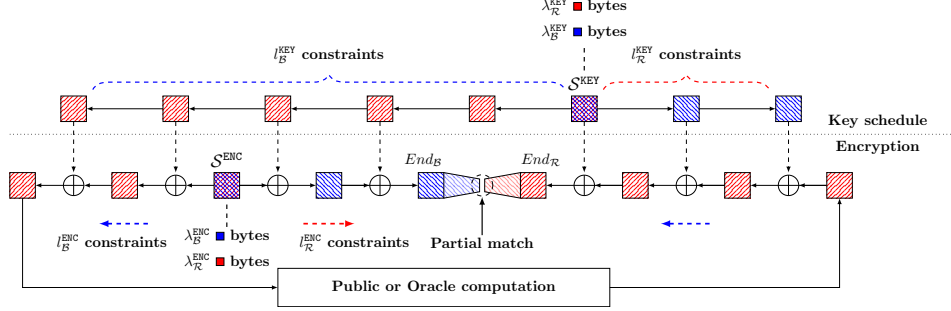


Fig. 1: A high-level overview of the MITM attacks [13]

148 requiring the full states, the partial matching exploits the filtering ability derived
 149 by the deterministic relation “ $End_B = End_R$ ” and denoted by d_m .

150 With the configurations of $(\lambda_B^{ENC}, \lambda_B^{KEY}, \lambda_R^{ENC}, \lambda_R^{KEY}, l_B^{ENC}, l_B^{KEY}, l_R^{ENC}, l_R^{KEY}, d_m)$, the
 151 basic attack procedure goes as follows:

- 152 1. Choose constants in \mathcal{S}^{ENC} and \mathcal{S}^{KEY} and $l_B^{ENC} + l_B^{KEY} + l_R^{ENC} + l_R^{KEY}$ constraints.
- 153 2. For 2^{d_B} values of \blacksquare neutral space, compute forward to End_B from the starting
 154 states, and store the values of \blacksquare in table $L_B[End_B]$.
- 155 3. For 2^{d_R} values of \blacksquare neutral space, compute backward to End_R from the
 156 starting states, and store the values of \blacksquare in table $L_R[End_R]$.
- 157 4. According to the indices, check the match between L_B and L_R .
- 158 5. For the surviving pairs that pass the match, check for a full-state match.

159 *Complexity analysis.* The above steps 2-5 form a MitM *episode*. To find an h -bit
 160 full match, $2^{h-(d_B+d_R)}$ episodes are needed. Since each episode is performed with
 161 a time of $2^{\max\{d_B, d_R\}} + 2^{d_B+d_R-d_m}$, the total time complexity is:

$$2^{h-(d_B+d_R)} \cdot (2^{\max\{d_B, d_R\}} + 2^{d_B+d_R-d_m}) \approx 2^{h-\min\{d_B, d_R, d_m\}} \quad (1)$$

162 Apparently, a MitM characteristic is valid, if and only if $\min\{d_B, d_R, d_m\} \geq$
 163 1. For MitM key recovery attack, additional constraints must be fulfilled to
 164 ensure that the internal states in \mathcal{S}^{ENC} can be totally determined by \mathcal{S}^{KEY} . This is
 165 equivalent to using up the DoFs of \mathcal{S}^{ENC} , i.e., $\lambda_B^{ENC} - l_B^{ENC} = 0$ and $\lambda_R^{ENC} - l_R^{ENC} = 0$.
 166 Besides, there should exist only one type of neutral bit in the plaintext or
 167 ciphertext, and at least 1-bit constant in the plaintext or ciphertext to avoid
 168 using up the full codebook. In [6], Bao *et al.* encoded the type of each byte in
 169 AES with a pair of boolean variables:

- 170 1. $\blacksquare \mathcal{R}, (x, y) = (0, 1)$: Known byte only with backward computation.
- 171 2. $\blacksquare \mathcal{B}, (x, y) = (1, 0)$: Known byte only with forward computation.
- 172 3. $\blacksquare \mathcal{G}, (x, y) = (1, 1)$: Constant byte and known in both forward and backward
 173 computations.
- 174 4. $\square \mathcal{W}, (x, y) = (0, 0)$: Unknown byte in forward and backward computations.

Then, the propagation rules for XOR and MixColumns can be described as a system of inequalities based on the above definitions. A valid MitM characteristic is defined as a solution solved by the off-the-shelf MILP solvers, like Gurobi [15], with the objective function that maximizes the $\min\{d_B, d_R, d_m\}$. For the detailed MILP models of these propagation rules, please refer to [6] or Appendix A.

2.2 Enhanced Techniques

Table-based method solving non-linear constraints. Note that Equation (1) holds mostly when the constraints imposed on neutral bits can be solved in $O(1)$ time, such as linear equations. However, there are many practice MitM characteristics with non-linear constrained neutral bits, which can not be solved efficiently. In [13], Dong *et al.* proposed a precomputation method to compute the value of the constraints by enumerating the neutral bits. Specifically, after setting the value of constants in starting states, do as follows:

1. For $2^{\lambda_B^{\text{ENC}} + \lambda_B^{\text{KEY}}}$ values, compute the values of $l_B^{\text{ENC}} + l_B^{\text{KEY}}$ constraints (denoted by $\mathbf{c}_B \in \mathbb{F}_2^{l_B^{\text{ENC}} + l_B^{\text{KEY}}}$) and store the $\lambda_B^{\text{ENC}} + \lambda_B^{\text{KEY}}$ bits in $U[\mathbf{c}_B]$.
2. For $2^{\lambda_R^{\text{ENC}} + \lambda_R^{\text{KEY}}}$ values, compute the values of $l_R^{\text{ENC}} + l_R^{\text{KEY}}$ constraints (denoted by $\mathbf{c}_R \in \mathbb{F}_2^{l_R^{\text{ENC}} + l_R^{\text{KEY}}}$) and store the $\lambda_R^{\text{ENC}} + \lambda_R^{\text{KEY}}$ bits in $V[\mathbf{c}_R]$.

Then, in each MitM episode, for a given \mathbf{c}_B and \mathbf{c}_R , the values in $U[\mathbf{c}_B]$ and $V[\mathbf{c}_R]$ can be searched in time $O(1)$. The time and memory cost for one precomputation phase are both $2^{\lambda_B^{\text{ENC}} + \lambda_B^{\text{KEY}}} + 2^{\lambda_R^{\text{ENC}} + \lambda_R^{\text{KEY}}}$.

SupP States and BiDir. In the SupP MitM framework of [7], neutral cells from both directions can be separated into two virtual states, called SupP states, to keep the linearity through linear operations. Then, \blacksquare and \blacksquare will be treated independently through linear operations, and the initial DoFs can be consumed in both directions. After a series of linear operations, two SupP states are finally combined before the next nonlinear operation. The color patterns and how the states are separated and combined are visualized in Figure 2. BiDir allows neutral cells to be consumed in both two directions, but this may lead to dependency between one type of neutral cell with non-linear constraints imposed on another. In [11], Degré proposed a more generic table-based method to cancel this dependency. Combined with the SupP states and BiDir methods, the solution space is greatly enlarged, such that some attack configurations with lower time complexities may be found. In the rest of this paper, we simplify the representation of SupP states. The virtual states of pure $\blacksquare/\blacksquare/\blacksquare/\blacksquare$ are omitted. And we denote the SupP states by the \blacksquare cell in which the blue cell and red cell occur simultaneously.

3 New Models for Linear Layer with Binary Matrix

In this section, we first propose an effective method to build an MILP model to describe the MitM attributes propagation through a n-XOR operation with SupP

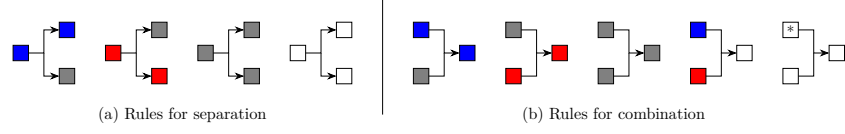


Fig. 2: Rules for separation and combination, where “*” means any color

states. Interestingly, the number of input cells involved in the **XOR** operation can be arbitrary, but the size of MILP model will not increase. However, we also observe that this may lead to double counting of constraints on the same neutral cells. Then, we show that the inaccuracy can be easily eliminated by adding an additional check model.

3.1 N-XOR Model

To simulate the MitM attributes propagation through the linear layer, Bao *et al.* proposed the **MC-RULE** for the MDS matrix in AES-like hashing [6,7]. As shown in Figure 3(a), each input cell has an effect on all output cells in MDS matrix. However, some primitives adopt a binary matrix in the diffusion layer where each output cell is computed by the **XOR** of partial input cells. As the Midori64’s binary matrix shown in Figure 3(b), the first output cell is only related to the last three input cells. Apparently, this will lead to inaccurate propagation if we apply the **MC-RULE** for MDS matrix on binary matrix directly since one output cell is not related to all input cells.

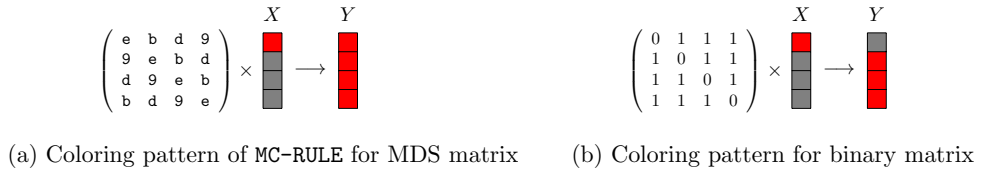


Fig. 3: A case of the difference of color pattern between MDS and binary matrix

In [13], Dong *et al.* proposed the **3-XOR-RULE** to model the key addition in **SKINNY- $n-3n$** . By enumerating four input cells, one output cell and one indicator variable for DoF cost, all valid color patterns can be restricted to a subset of \mathbb{F}_2^{11} , which can be described into a system of inequalities using the convex hull technique [36]. If we directly extend the strategy of **3-XOR-RULE** to the **XOR** operation with n input cells, then the enumeration scope will be restricted to a subset of \mathbb{F}_2^{2n+3} . When n is large, it’s complicated and error-prone to enumerate all valid color patterns. And the size of the system of inequalities may be large, which renders the model infeasible to compute.

238 An alternative strategy is to apply the XOR-RULE in [6,7] for two-input XOR
 239 consecutively. This strategy is valid but may miss some valid patterns by intro-
 240 ducing additional auxiliary variables. We take the attribute propagation through
 241 Midori64's diffusion layer to state this fact as shown in Figure 4. In the first step
 242 of Figure 4(a), an auxiliary variable `auxi` is needed to carry on the output of
 243 $X[2] \oplus X[3]$. For the second step, $X[1]$ and $X[0]$ are XORed with `auxi` to compute
 244 $Y[0]$ and $Y[1]$, respectively. Then, one of the following cases will occur,

- 245 – If `auxi` is ■ by consuming one DoF, then $Y[0]$ will always be ■, and $Y[1]$
 246 will always be ■.
- 247 – If `auxi` is ■, then $Y[1]$ will always be ■. $Y[0]$ can be either ■ or ■ by consuming
 248 one DoF.

249 However, with the n-XOR model in Figure 4(b), step 1 and step 2 can be exe-
 250 cuted independently without correlated variables. Then, $Y[0]$ and $Y[1]$ can be
 251 ■ simultaneously by consuming 2 DoFs of ■, which can not be captured by the
 first strategy.

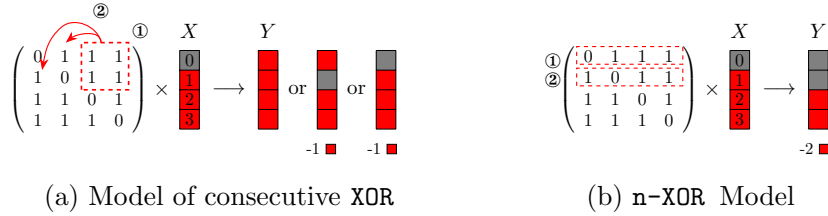


Fig. 4: The advantage of n-XOR model compared with consecutive XOR

252 In the following, we show how to convert the propagation of ■ cells through
 253 the n-XOR operation under SupP states into MILP language. All coloring pat-
 254 terns can be specified by the following set of rules denoted by n-XOR-RULE⁻.
 255 The n-XOR-RULE⁺ for ■ can be obtained in a similar way by exchanging ■ and
 256 ■ since they are dual.

- 258 – n-XOR-RULE⁻-1. If there is at least one ■ in input, then the output is ■.
- 259 – n-XOR-RULE⁻-2. If all cells of the input are ■, then the output must be ■.
- 260 – n-XOR-RULE⁻-3. If there are ■ and ■ cells but no ■ cell in the input, then
 261 one of the following situations will occur:
 - 262 • The output is ■ cell and no DoF is consumed.
 - 263 • The output is ■ by consuming one DoF of ■.

264 Let $(A[1], A[2], \dots, A[n])$ be the input of n-XOR where $A[i] = (x_i^A, y_i^A)$. Let B be
 265 the output where $B = (x^B, y^B)$. Like [6], we introduce three boolean indicator
 266 variables μ, ν and η in the model. $\mu = 1$ if and only if there exists $i \in [1, 2, \dots, n]$
 267 such that $(x_i^A, y_i^A) = (0, 0)$. That is, n-XOR-RULE⁻-1 is fulfilled. $\nu = 1$ if and only
 268 if $x_i^A = y_i^A = 1$ for all $1 \leq i \leq n$, which corresponds to n-XOR-RULE⁻-2. When

269 $\mu = \nu = 0$, **n-XOR-RULE**⁻-3 is fulfilled. Besides, $\eta = 1$ when there exists one
 270 constraint imposed on input \blacksquare cells. With the help of indicator variables, the
 271 **n-XOR-RULE**⁻ can be converted into a system of inequalities shown in Equation
 (2) and Equation (3).

$$\begin{aligned}
 & \left\{ \begin{array}{l} \sum_{i=0}^{n-1} y_i^A + \mu \leq n \\ \sum_{i=0}^{n-1} y_i^A + n \cdot \mu \geq n \\ \sum_{i=0}^{n-1} x_i^A - \nu \leq n - 1 \\ \sum_{i=0}^{n-1} x_i^A - n \cdot \nu \geq 0 \end{array} \right. \quad (2) \quad \left\{ \begin{array}{l} y^B + \mu = 1 \\ x^B + \mu \leq 1 \\ \eta - x^B + \nu = 0 \\ \sum_{i=0}^{n-1} x_i^A + x^B - 2 \cdot \nu \leq n - 1 \\ \sum_{i=0}^{n-1} x_i^A + x^B - (n + 1) \cdot \nu \geq 0 \end{array} \right. \quad (3)
 \end{aligned}$$

272 At the end, we must emphasize that, in addition to preserving more valid
 273 coloring patterns, another advantage of **n-XOR** is that the size of model is fixed,
 274 independent of the number of input cells. And this makes it possible to de-
 275 scribe the attributes propagation for primitives with large binary matrices, like
 276 **Camellia** and **Aria**.
 277

278 3.2 Check Model: More Accurate Consumption of DoFs

279 We also observe that **n-XOR** model may lead to some subtle inaccuracies. We still
 280 take a possible propagation of **Midori64**'s diffusion layer as an example to state
 281 this fact. A particularly explicit case is that the constraint on the same neutral
 282 cells may be double counted due to the independent computation of each output
 283 cell as shown in Figure 5(a). Besides, there are some more implicit cases leading
 284 to inaccuracy as shown in Figure 5(b).

285 Then, we introduce the check model to show how the inaccuracy can be
 286 eliminated, and describe it in the MILP language. We still state this by con-
 287 sidering the \blacksquare propagation through the **n-XOR** operation under SupP states. Let
 288 $A[j] = (x_j^A, y_j^A)$, for $1 \leq j \leq n$, be the input of the $n \times n$ binary matrix M .
 289 After the **n-XOR** Model, we can get $\eta = (\eta_1, \dots, \eta_n)$ denoted by the degree con-
 290 sumption vector where η_i is the indicator variable introduced in Equation (3)
 291 and $\eta_i = 1$ means there exists one constraint imposed on the input \blacksquare cells for the
 292 i -th row of M . Since only \blacksquare cells are needed to be considered for DoF consump-
 293 tion, we introduce another $n \times n$ binary matrix M' to intuitively mark which \blacksquare
 294 cells contribute to the DoF consumption. Then, M' is generated as follows :

- 295 – If $\eta_i = 1$ and $M_{i,j} = 1$ and $x_j^A = 0$, then $M'_{i,j} = 1$.
- 296 – If the first case is not satisfied, then $M'_{i,j} = 0$.

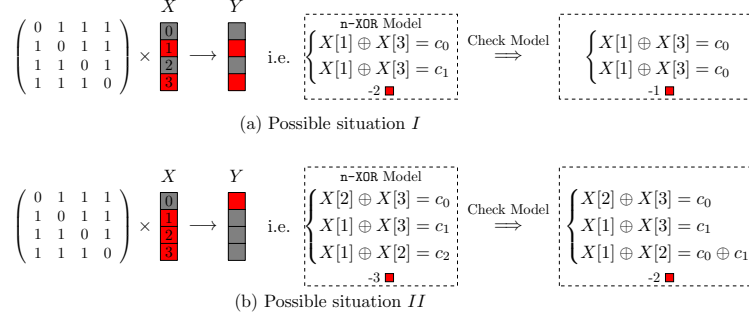


Fig. 5: Possible situations in our models

For the first case, $\eta_i = 1$ means no \square in the involved input cells, and $M_{i,j} = 1$ and $x_j^A = 0$ means $A[j]$ is a \blacksquare cell involved in the i -th XOR operation. We introduce a general variable η' to denote the rank of M' , which equals to the accurate DoF consumption theoretically. Since M is a fixed matrix, we can conclude that the accurate DoF consumption can be determined by the other $2n$ variables $(x_1^A, \dots, x_n^A, \eta_1, \dots, \eta_n)$. Finally, the subset $(x_1^A, \dots, x_n^A, \eta_1, \dots, \eta_n, \eta')$ of $\mathbb{F}_2^{2n} \times \mathbb{F}_{n+1}$ can be restricted to a system of linear inequalities using the convex hull technique [36]. Different with the origin framework, the configuration $l_{\mathcal{R}}^{\text{ENC}} + l_{\mathcal{R}}^{\text{KEY}}$ should be calculated by accumulating the accurate DoF consumption determined by the **n-XOR** and check model, along with extra constraints imposed by other operations, such as **KeyAddition**. The configuration $l_{\mathcal{B}}^{\text{ENC}} + l_{\mathcal{B}}^{\text{KEY}}$ for degree consumption of \blacksquare can also be gotten in the similar way due to the duality [7].

However, it should be noted that the cost of exhaustion to determine the accurate DoF consumption is still affected by the number of input cells. Hence, check model can not be applied to large binary matrix ($n > 4$ in this paper). Although it's trivial to compute the rank of a general matrix in $O(n^3)$, there is still no effective way to implement it in MILP model. Besides, in addition to finding out better modeling methods or more suitable optimizers, we can still combine theoretical models and manually checking to deal with large matrices, such as Section 5 and Section 6. In practice, by relaxing the constraint to $\min\{d_{\mathcal{B}}, d_{\mathcal{R}}, d_m\} \geq 1 - i$, where $i \geq 1$, we check the feasible solutions to find out valid characteristic. It also should be noted that the final results derived by the manually checking method may not be the optimal solution.

4 MitM Key Recovery Attack on Midori64

Midori64 is an SPN-based lightweight block cipher, consisting of 64-bit block and a 128-bit key. The state is seen as a 4×4 matrix of 4-bit cells, and its diffusion layer is 4×4 boolean matrix. The detailed specification is provided in Appendix B.1.

In this section, we present an 11-round MitM key recovery attack on Midori64 with a time complexity of 2^{124} . For the weakened version of Midori64, without

whitening key, a 12-round MitM characteristic is found with a time complexity of 2^{120} . Despite a little higher time complexity, the above two attacks can be applied with extremely low data and memory cost compared to the previous best work [23,35]. Besides, the data and memory of the attack on 12-round weakened Midori64 can be further reduced if the time complexity is relaxed to 2^{124} .

4.1 MitM Key Recovery Attack on 11-round Midori64

As shown in Figure 6 and Figure 7, an 11-round MitM key recovery attack is identified, where $|\mathcal{S}^{\text{ENC}}| = 16$ independent bytes in the encryption data path are set to be 0 as Line 1-2 in Algorithm 1, to ensure the values of all the other bytes are totally determined by the given key. And at least one 0 byte in the ciphertext C to avoid using the full codebook. The starting states are C and $(K^{(0)}, K^{(1)})$. The encryption data path provides $\lambda_{\mathcal{R}}^{\text{ENC}} = 9$ and $\lambda_{\mathcal{B}}^{\text{ENC}} = 0$ DoFs for \blacksquare and \blacksquare , respectively. And the $\lambda_{\mathcal{R}}^{\text{ENC}} = 9$ \blacksquare cells are used up when computing $A_{\text{Shc}}^{(9)}$ through an MC operation and $A_{\text{MC}}^{(8)}$ through an XOR operation in the backward computation path. For $(K^{(0)}, K^{(1)})$, the initial DoFs for \blacksquare and \blacksquare are $\lambda_{\mathcal{R}}^{\text{KEY}} = 3$ and $\lambda_{\mathcal{B}}^{\text{KEY}} = 2$, respectively. In the key schedule, $K^{(0)}[1] \oplus K^{(0)}[9]$ and $K^{(0)}[1] \oplus K^{(0)}[13]$ are restricted to constants, i.e., $l_{\mathcal{R}}^{\text{KEY}} = 2$. Hence, we get $\text{DoF}_{\mathcal{R}} = \lambda_{\mathcal{R}}^{\text{KEY}} - l_{\mathcal{R}}^{\text{KEY}} = 1$. Similarly, $K^{(0)}[5] \oplus K^{(1)}[5]$ is imposed on $l_{\mathcal{B}}^{\text{KEY}} = 1$ constraint, and then $\text{DoF}_{\mathcal{B}} = \lambda_{\mathcal{B}}^{\text{KEY}} - l_{\mathcal{B}}^{\text{KEY}} = 1$. The matching phase happens at the MC operation between $A_{\text{Shc}}^{(3)}$ and $A_{\text{MC}}^{(3)}$, providing $d_m = 1$ degree of matching by Equation (4).

$$A_{\text{Shc}}^{(3)}[2] \oplus A_{\text{Shc}}^{(3)}[10] = A_{\text{MC}}^{(3)}[2] \oplus A_{\text{MC}}^{(3)}[10] \quad (4)$$

According to Equation (1), the overall time complexity is $2^{4 \times (32 - \min\{1,1,1\})} \approx 2^{124}$. The data complexity is 2^{36} by traversing the $16 - 7 = 9$ non-constant cells in C . A detailed attack procedure is given in Algorithm 1. The memory cost is about 2^6 bytes to store $(\mathcal{S}_{\mathcal{R}}, \mathcal{S}_{\mathcal{B}}, L)$.

4.2 MitM Key Recovery Attack on 12-round Weakened Midori64

In this section, we focus on the weakened version of Midori64 omitting the whitening layers. And we found a MitM key recovery attack on the 12-round Midori64 as shown in Figure 8. As explained above, $|\mathcal{S}^{\text{ENC}}| = 16$ independent \blacksquare bytes in the encryption data path are set as 0. The starting states are ciphertext C and two sub-key $(K^{(0)}, K^{(1)})$. In ciphertext, there are $\lambda_{\mathcal{R}}^{\text{ENC}} = 12$ and $\lambda_{\mathcal{B}}^{\text{ENC}} = 0$ initial DoFs for \blacksquare and \blacksquare , respectively. And the DoFs of \blacksquare are used up when computing $A_{\text{Shc}}^{(10)}$ through an MC operation and $A_{\text{MC}}^{(9)}$ through an XOR operation. The two sub-key $(K^{(0)}, K^{(1)})$ provide $\lambda_{\mathcal{R}}^{\text{KEY}} = 6$ and $\lambda_{\mathcal{B}}^{\text{KEY}} = 2$ initial DoFs for \blacksquare and \blacksquare , respectively. For the key schedule, $K^{(0)}[0] \oplus K^{(0)}[4]$, $K^{(0)}[0] \oplus K^{(0)}[8]$, $K^{(0)}[1] \oplus K^{(0)}[5]$ and $K^{(0)}[1] \oplus K^{(0)}[13]$ are restricted to constants, i.e., $l_{\mathcal{R}}^{\text{KEY}} = 4$. Hence, we get $\text{DoF}_{\mathcal{R}} = \lambda_{\mathcal{R}}^{\text{KEY}} - l_{\mathcal{R}}^{\text{KEY}} = 2$ and $\text{DoF}_{\mathcal{B}} = \lambda_{\mathcal{B}}^{\text{KEY}} = 2$. The matching phase happens at the MC operation between $A_{\text{Shc}}^{(4)}$ and $A_{\text{MC}}^{(4)}$, providing $d_m = 1$

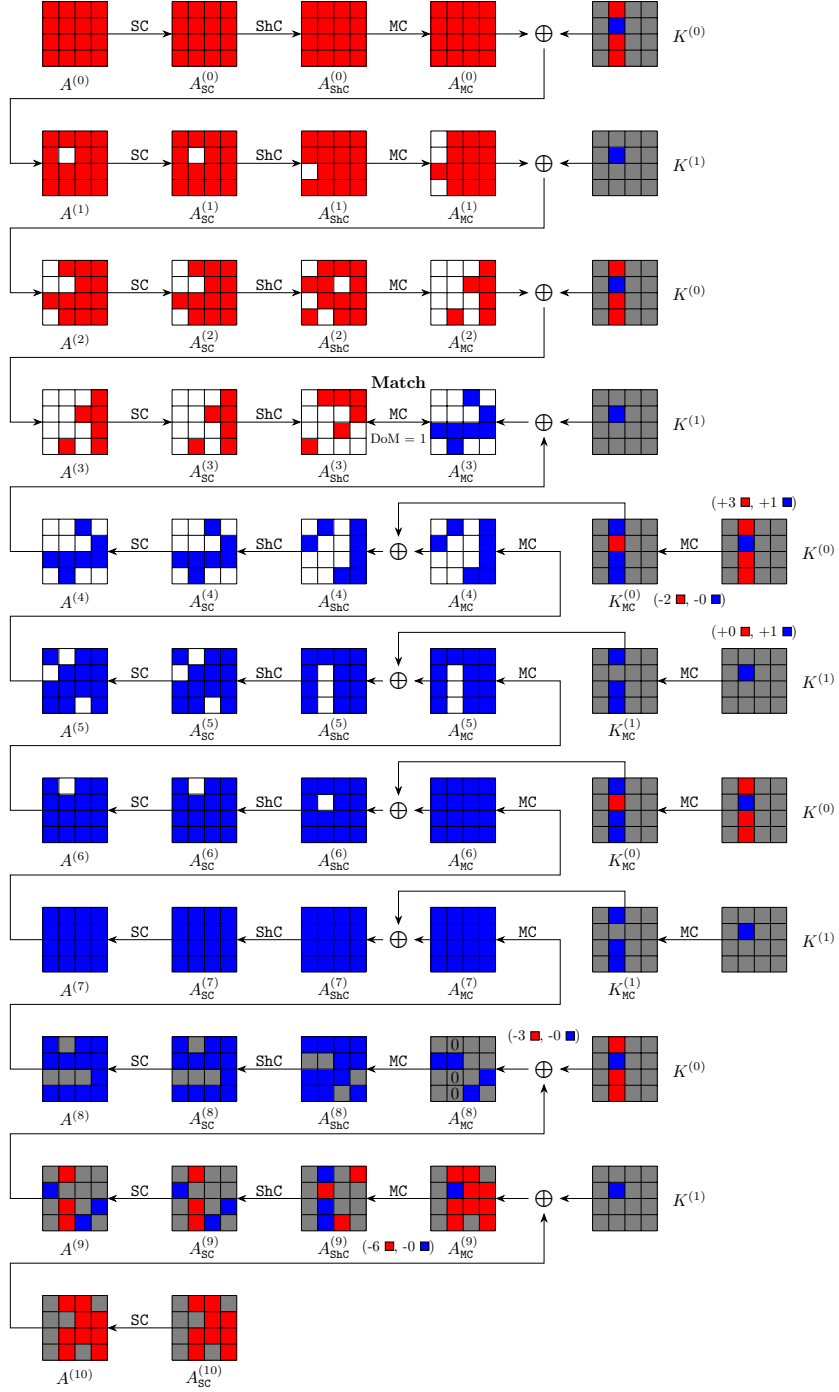


Fig. 6: Meet-in-the-Middle key recovery attack on 11-round Midori64

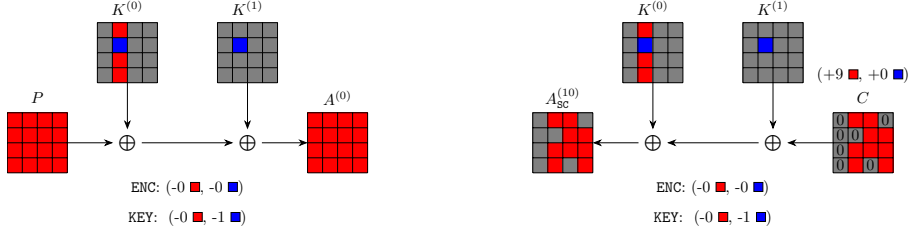


Fig. 7: The MitM characteristic through whitening layers of 11-round Midori64

Algorithm 1: MitM Key Recovery Attack on 11-round Midori64

```

1 Set the  $\blacksquare$  bytes to be 0, i.e.,  $C[0, 3, 4, 5, 8, 12, 14] \leftarrow 0$ ,  $A_{\text{MC}}^{(8)}[1, 9, 13] \leftarrow 0$ 
2  $A_{\text{MC}}^{(9)}[1] \oplus A_{\text{MC}}^{(9)}[9] \leftarrow 0$ ,  $A_{\text{MC}}^{(9)}[1] \oplus A_{\text{MC}}^{(9)}[13] \leftarrow 0$ ,  $A_{\text{MC}}^{(9)}[2] \oplus A_{\text{MC}}^{(9)}[6] \leftarrow 0$ ,
    $A_{\text{MC}}^{(9)}[2] \oplus A_{\text{MC}}^{(9)}[10] \leftarrow 0$ ,  $A_{\text{MC}}^{(9)}[7] \oplus A_{\text{MC}}^{(9)}[11] \leftarrow 0$ ,  $A_{\text{MC}}^{(9)}[7] \oplus A_{\text{MC}}^{(9)}[15] \leftarrow 0$ 
3 Collecting plaintext-ciphertext pairs by traversing the non-constant  $16 - 7 = 9$ 
   cells in  $C$ , and storing them in table  $H$ 
4 for all possible values of the  $\blacksquare$  cells in  $K^{(0)}$  and  $K^{(1)}$  do
5    $A_{\text{SC}}^{(10)}[0, 3, 4, 5, 8, 12, 14] \leftarrow (K^{(0)} \oplus K^{(1)})[0, 3, 4, 5, 8, 12, 14]$ 
6   for  $(\mathbf{c}_{\mathcal{R},1}, \mathbf{c}_{\mathcal{R},2}, \mathbf{c}_{\mathcal{B}}) \in \mathbb{F}_2^{3 \times 4}$  do
7     Derive the solution space  $\mathcal{S}_{\mathcal{R}}$  of  $\blacksquare$  cells by
           
$$\begin{cases} K^{(0)}[1] \oplus K^{(0)}[9] = \mathbf{c}_{\mathcal{R},1} \\ K^{(0)}[1] \oplus K^{(0)}[13] = \mathbf{c}_{\mathcal{R},2} \end{cases}$$

8     Derive the solution space  $\mathcal{S}_{\mathcal{B}}$  of  $\blacksquare$  cells by  $K^{(0)}[5] \oplus K^{(1)}[5] = \mathbf{c}_{\mathcal{B}}$ 
9      $L \leftarrow []$ 
10    for  $v_{\mathcal{R}} \in \mathcal{S}_{\mathcal{R}}$  do
11      Compute  $A_{\text{ShC}}^{(3)}[2, 10]$  along the forward computation path:
12       $A_{\text{MC}}^{(8)} \rightarrow C \rightarrow \text{Dec}_K(C) \rightarrow A_{\text{ShC}}^{(3)}$  by accessing  $H$ 
13       $L[A_{\text{ShC}}^{(3)}[2] \oplus A_{\text{ShC}}^{(3)}[10]] \leftarrow v_{\mathcal{R}}$ 
14    end
15    for  $v_{\mathcal{B}} \in \mathcal{S}_{\mathcal{B}}$  do
16      Compute  $A_{\text{MC}}^{(3)}[2, 10]$  along the backward computation path:
17       $C \rightarrow A_{\text{MC}}^{(3)}$ 
18      for Candidate keys in  $L[A_{\text{MC}}^{(3)}[2] \oplus A_{\text{MC}}^{(3)}[10]]$  do
19        Test the guessed key with several plaintext-ciphertext pairs
20      end
21    end
22 end

```

364 degree of matching by Equation (5).

$$A_{\text{Shc}}^{(4)}[4] \oplus A_{\text{Shc}}^{(4)}[12] = A_{\text{Mc}}^{(4)}[4] \oplus A_{\text{Mc}}^{(4)}[12] \quad (5)$$

365 In [14], Fuhr *et al.* proposed the *simultaneous matching* to decrease $2^{d_B+d_R-d_m}$ in
 366 Equation (1) exponentially by testing the surviving keys with multiple plaintext-
 367 ciphertext pairs in parallel. Hence, the overall time is dominated by $2^{4 \times (32 - \min\{2,2\})} \approx$
 368 2^{120} . The data complexity is 2^{48} by traversing the $16 - 4$ non-constant cells in C .
 369 A detailed attack procedure is given in Algorithm 2. The memory cost is $2^{10.6}$
 370 bytes to store (\mathcal{S}_R, L) .

371 When considering optimization for data complexity, we found a MitM key
 372 recovery attack on 12-round Midori64 with data complexity of 2^{36} by relaxing
 373 the time complexity to 2^{124} . The figure and algorithm are given in Figure 17
 374 and Algorithm 4 in Appendix C.

Algorithm 2: MitM Key Recovery Attack on 12-round weakened Midori64, optimized for time complexity

```

1  $C[2, 6, 10, 14] \leftarrow 0, A_{\text{Shc}}^{(10)}[1, 4, 7, 9, 12, 15] \leftarrow 0, A_{\text{Mc}}^{(9)}[0, 1, 4, 5, 8, 13] \leftarrow 0$ 
2 Collecting plaintext-ciphertext pairs by traversing the non-constant
    $16 - 4 = 12$  cells in  $C$ , and storing them in table  $H$ 
3 for all possible values of the  $\blacksquare$  cells in  $K^{(0)}$  and  $K^{(1)}$  do
4   for  $(c_{R,1}, c_{R,2}, c_{R,3}, c_{R,4}) \in \mathbb{F}_2^{4 \times 4}$  do
5     Derive the solution space  $\mathcal{S}_R$  of  $\blacksquare$  cells by
        
$$\begin{cases} K^{(0)}[0] \oplus K^{(0)}[4] = c_{R,1} & K^{(0)}[0] \oplus K^{(0)}[8] = c_{R,2} \\ K^{(0)}[1] \oplus K^{(0)}[5] = c_{R,3} & K^{(0)}[1] \oplus K^{(0)}[13] = c_{R,4} \end{cases}$$

6      $L \leftarrow []$ 
7     for  $v_R \in \mathcal{S}_R$  do
8       Compute  $A_{\text{Shc}}^{(4)}[4, 12]$  along the forward computation path:
9        $A_{\text{Mc}}^{(9)} \rightarrow C \rightarrow \text{Dec}_K(C) \rightarrow A_{\text{Shc}}^{(4)}$  by accessing  $H$ 
10       $L[A_{\text{Shc}}^{(4)}[4] \oplus A_{\text{Shc}}^{(4)}[12]] \leftarrow v_R$ 
11    end
12    for  $2^{2 \times 4}$  possible values of  $K^{(1)}[7, 12]$  do
13      Compute  $A_{\text{Mc}}^{(4)}[4, 12]$  along the backward computation path:
         $C \rightarrow A_{\text{Mc}}^{(4)}$ 
14      for Candidate keys in  $L[A_{\text{Mc}}^{(4)}[4] \oplus A_{\text{Mc}}^{(4)}[12]]$  do
15        Test the guessed key with several plaintext-ciphertext pairs
16      end
17    end
18  end
19 end
```

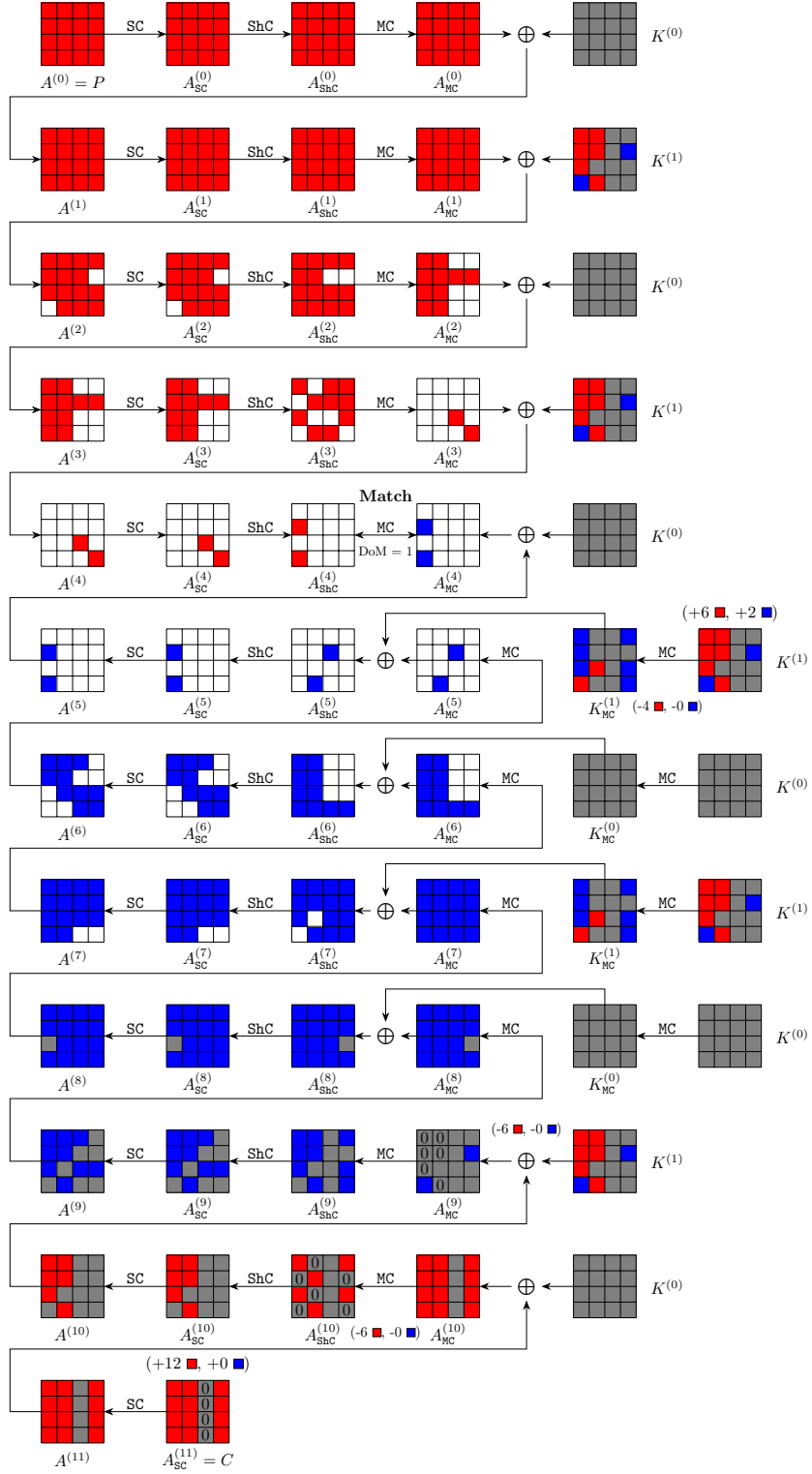


Fig. 8: Meet-in-the-Middle key recovery attack on 12-round weakened Midori64, optimized for time complexity

5 MitM Preimage Attack on Weakened Camellia

Camellia is a Feistel-based block cipher with 128-bit block. The state is represented as 8 cells of 8-bit. the diffusion layer is a 8×8 boolean matrix. In this work, we only target on the version with a 128-bit key. The detailed specification is provided in Appendix B.2.

5.1 The MitM Characteristic of 14-round weakened Camellia

We first applied the n-XOR model to describe the attributes propagation through the diffusion layer. However, the check model can not be deployed since the large size of the diffusion layer. We relaxed the constraint to $\min\{d_B, d_R, d_m\} \geq 1 - i$, where $i \geq 1$, as stated in Section 3.2, and manually checked the solution files to find out valid solutions (may not be optimal).

The final valid configuration of the pseudo-preimage MitM attack on 14-round weakened **Camellia**-MM0 without FL/FL^{-1} and whitening layers is shown in Figure 9. We deploy the n-XOR model by considering the MixColumns and XOR as a whole. The attack starts at $A^{(9)}$ and $B^{(9)}$ illustrated in Figure 9(a), in which the initial DoFs for \blacksquare and \blacksquare are $\lambda_B = \lambda_R = 7$. In the forward computation path, in order to facilitate the propagation of \blacksquare cells, there are $l_R = 6$ linear constraints imposed on $A_{SB}^{(9)}[7] \oplus B^{(9)}[i]$, for $i \in \{0, 1, 2, 4, 5, 6\}$. Similarly, in the backward computation path, $l_B = 6$ linear constraints are imposed on $A_{SB}^{(8)}[7] \oplus A^{(9)}[i]$, for $i \in \{0, 1, 2, 4, 5, 6\}$, to facilitate the propagation of \blacksquare cells. Hence, we get $d_B = \lambda_B - l_B = 1$ and $d_R = \lambda_R - l_R = 1$.

Around the feed-forward mechanism of MM0 mode, we set global constraints on round keys $(k_0, k_1, k_{12}, k_{13})$ to preserve some attributes like [28]. Specifically, for the given target $H_0 \| H_1$, $A_{SB}^{(0)}$ equals to $A_{SB}^{(13)}$ by setting $k_0 = k_{13} \oplus H_0$ globally. Since $B^{(0)} = MC(A_{SB}^{(13)}) \oplus A^{(12)} \oplus H_1$ and $A^{(1)} = B^{(0)} \oplus MC(A_{SB}^{(0)})$, then we can get $A^{(1)} = A^{(12)} \oplus H_1$. Similarly, $A^{(2)}$ equals to $B^{(12)} \oplus H_0$ by setting $k_1 = k_{12} \oplus H_1$. The cost to determine such proper subkeys is given in Section 5.2 and will not exceed the time complexity of main MitM procedure.

The matching points are $A^{(5)}$ and $B^{(5)}$ in Figure 9(c). At first glance, there are no degree for the direct matching. However, after applying a linear transformation P^{-1} to $B^{(5)}$ as in Figure 10, two-byte degree of match are derived. Since $d_B = d_R = 1$, we only use one-byte for match, i.e., $d_m = 1$. The specific matching equation is Equation (6).

$$\bigoplus_{i \in [0, 1, 2, 4, 5, 6]} \blacksquare^{(3)}[i] \oplus A_{SB}^{(3)}[3] = \bigoplus_{i \in [0, 1, 2, 4, 5, 6]} \blacksquare^{(6)}[i] \oplus A_{SB}^{(5)}[3] \quad (6)$$

According to Equation (1), the total time complexity is bounded by $2^{8 \times (16 - \min\{1, 1, 1\})} \approx 2^{120}$. A detailed attack procedure is given in Algorithm 3. The memory complexity of a hash table L is 2^8 . And this attack can be converted to a second preimage attack with a time complexity of 2^{125} according to [24, Fact9.99].

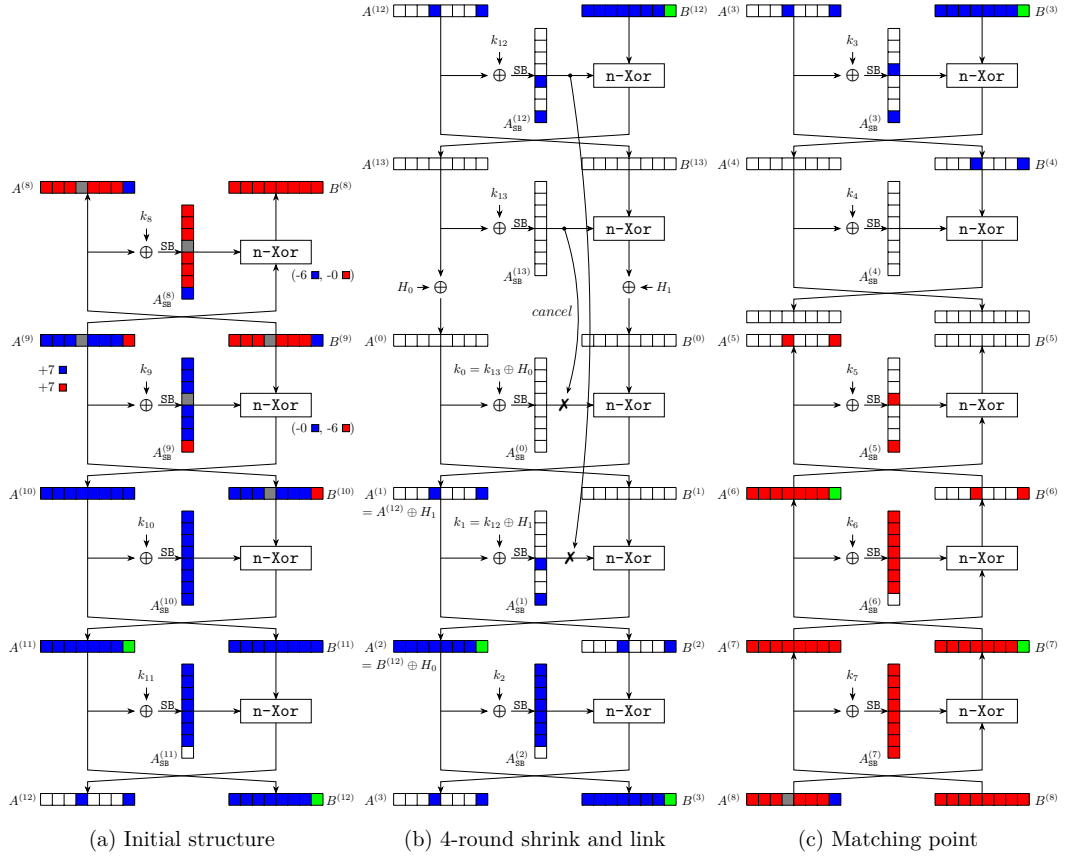


Fig.9: Meet-in-the-Middle pseudo-preimage attack on 14-round weakened Camellia-MMO

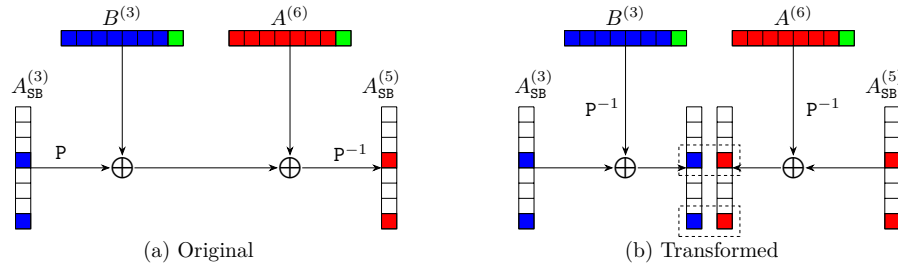


Fig.10: The matching process of 14-round weakened Camellia-MMO

Algorithm 3: MitM Pseudo-Preimage Attack on 14-round weakened Camellia-MM0

```

1  Setting a global key satisfying  $k_0 = k_{13} \oplus H_0$ ,  $k_1 = k_{12} \oplus H_1$ ;
2  for  $2^{16}$  values of the  $\blacksquare$  bytes in  $A^{(9)}[3]||B^{(9)}[3]$  do
3      for  $\mathbf{c}_B \in \mathbb{F}_2^{8 \times 6}$  do
4          for  $\mathbf{c}_R \in \mathbb{F}_2^{8 \times 6}$  do
5               $L \leftarrow []$ 
6              Solve the following system of equations to find the solution space
7                   $\mathcal{S}_B$  of  $\blacksquare$  in  $A^{(9)}$  and  $B^{(9)}$ ; /*  $|\mathcal{S}_B| = 2^{8 \times (7-6)} = 2^8$  */

               $A_{\text{SB}}^{(8)}[7] \oplus A^{(9)}[0] = \mathbf{c}_B[0]$ ,  $A_{\text{SB}}^{(8)}[7] \oplus A^{(9)}[1] = \mathbf{c}_B[1]$ ,  $A_{\text{SB}}^{(8)}[7] \oplus A^{(9)}[2] = \mathbf{c}_B[2]$ ,
               $A_{\text{SB}}^{(8)}[7] \oplus A^{(9)}[4] = \mathbf{c}_B[3]$ ,  $A_{\text{SB}}^{(8)}[7] \oplus A^{(9)}[5] = \mathbf{c}_B[4]$ ,  $A_{\text{SB}}^{(8)}[7] \oplus A^{(9)}[6] = \mathbf{c}_B[5]$ .

8              Solve the following system of equations to find the solution space
9                   $\mathcal{S}_R$  of  $\blacksquare$  in  $A^{(9)}$  and  $B^{(9)}$ ; /*  $|\mathcal{S}_B| = 2^{8 \times (7-6)} = 2^8$  */

               $A_{\text{SB}}^{(9)}[7] \oplus B^{(9)}[0] = \mathbf{c}_R[0]$ ,  $B_{\text{SB}}^{(9)}[7] \oplus A^{(9)}[1] = \mathbf{c}_R[1]$ ,  $A_{\text{SB}}^{(9)}[7] \oplus B^{(9)}[2] = \mathbf{c}_R[2]$ ,
               $A_{\text{SB}}^{(9)}[7] \oplus B^{(9)}[4] = \mathbf{c}_R[3]$ ,  $A_{\text{SB}}^{(9)}[7] \oplus B^{(9)}[5] = \mathbf{c}_R[4]$ ,  $A_{\text{SB}}^{(9)}[7] \oplus B^{(9)}[6] = \mathbf{c}_R[5]$ .

10             for  $v_B \in \mathcal{S}_B$  do
11                 Compute forward to  $A^{(3)}$  and  $B^{(3)}$ , derive 1-byte  $End_B$  by
12                      $End_B \leftarrow P^{-1}(B^{(3)})[3] \oplus A_{\text{SB}}^{(3)}[3]$ 
13                  $L[End_B] \leftarrow v_B$ ;
14             end
15             for  $v_R \in \mathcal{S}_R$  do
16                 Compute backward to  $A^{(6)}$  and  $B^{(6)}$ , derive 1-byte  $End_R$  by
17                      $End_R \leftarrow P^{-1}(A^{(6)})[3] \oplus A_{\text{SB}}^{(5)}[3]$ 
18                 for  $v_B \in L[End_R]$  do
19                     Reconstruct the (candidate) message  $X$ ;
20                     /*  $2^{8 \times (1+1-1)} = 2^8$  values passed the filter */
21                     if  $X$  is a preimage then
22                         Output  $X$  and stop;
23                     end
24                 end
25             end
26         end
27     end

```

412 5.2 The Cost to Determine a Proper Key

413 The key schedule of **Camellia** with 128-bit key is shown in Figure 15. As ex-
414 plained above, we only need to focus on $(k_0, k_1, k_{12}, k_{13})$ [1],

$$k_0 \leftarrow K'_A, \quad k_1 \leftarrow K''_A, \quad k_{12} \leftarrow K''[30-63] \parallel K'[0-29], \quad k_{13} \leftarrow K'[30-63] \parallel K''[0-29].$$

415 As shown in Figure 15, every internal state can be derived for given K' and
416 S_0 . Hence, we get $K'' = F_0(K') \oplus S_0$ and $K''_A = F_2(F_1(S_0)) \oplus F_0(K')$. According
417 to the global constraints $k_0 = k_{13} \oplus H_0$ and $k_1 = k_{12} \oplus H_1$, the relation between
418 K' and S_0 can be represented as Equation (7).

$$F_2(F_1(S_0)) \oplus F_0(K') = (F_0(K') \oplus S_0)[30-63] \parallel K'[0-29] \oplus H_1 \quad (7)$$

419 Besides, we note that K' and S_0 can be placed at two sides of Equation (8),
420 respectively. The left-hand-side of Equation (8) only contains variables in terms
421 of K' , while the right-hand-side of Equation (8) depends on S_0 .

$$F_0(K') \oplus F_0(K')[30-63] \parallel K'[0-29] = F_2(F_1(S_0)) \oplus S_0[30-63] \parallel \overbrace{0 \cdots 0}^{30} \oplus H_1 \quad (8)$$

422 Then, an algebraic meet-in-the-middle attack can be mounted by enumerating
423 K' and S_0 independently to filter out valid pairs according to Equation (8), i.e.
424 $d_B = d_R = d_m = 64$. The time and memory complexity are both 2^{64} . Besides,
425 the memory cost can be further reduced by extracting partial x bits of K' and
426 S_0 as global variables. Then, the memory can be reduced by a fraction of 2^x ,
427 while the total time is bounded by 2^{64+x} . To avoid exceeding the time cost of
428 main MitM procedure, $64 + x \leq 120$ should be fulfilled, i.e., x can take 56 at
429 most. The corresponding memory cost is 2^8 .

430 6 MitM Preimage Attack on 6-Round Aria

431 **Aria** is an SPN-based block cipher that supports a 128-bit block. In this work,
432 we target on the version with a 128-bit key. The state is treated as a 4×4 matrix.
433 And the diffusion layer is a 16×16 boolean matrix. The detailed specification
434 of **Aria** is presented in Appendix B.3.

435 Since the large size diffusion layer, only the **n-XOR** model can be applied
436 to describe the MitM attribution propagation through the diffusion layer. By
437 relaxing the constraint to $\min\{d_B, d_R, d_m\} \geq 1 - i$, where $i \geq 1$, as stated in
438 Section 3.2, we finally found out a valid configuration of the pseudo-preimage
439 MitM attack on 6-round **Aria-DM** as shown in Figure 11 (may not be optimal).
440 The attack starts at $A^{(1)}$ in which the initial DoFs for \blacksquare and \blacksquare are $\lambda_B = 1, \lambda_R =$
441 14 , respectively. Since there are non-linear constraints on \blacksquare cells to compute $A_{DL}^{(2)}$
442 through the DL operation. We use the table-based method in [13] to solve such
443 non-linear constraints.

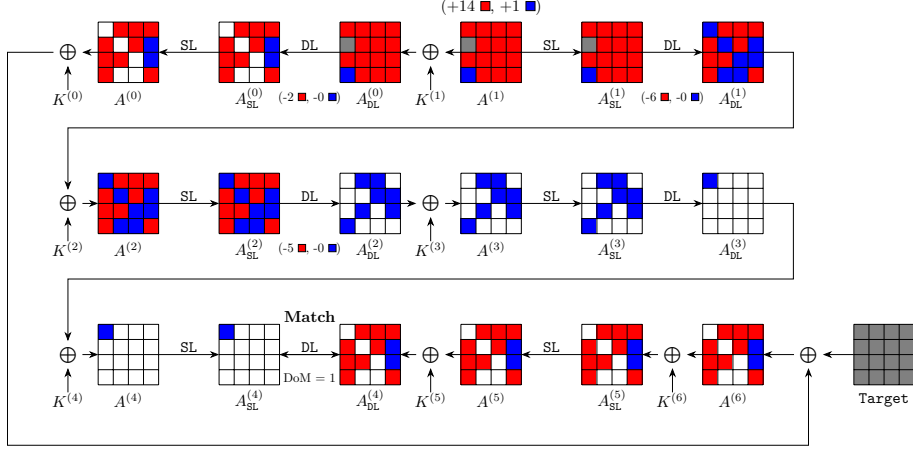


Fig. 11: Meet-in-the-Middle pseudo-preimage attack on 6-round Aria-DM

444 *Precomputation of red initial values.* By enumerating the ■ cells in $A^{(1)}$, in the
 445 backward computation path, two constraints imposed on ■ cells can be computed
 446 as follows:

$$\begin{cases} A_{\text{DL}}^{(0)}[0] \oplus A_{\text{DL}}^{(0)}[6] \oplus A_{\text{DL}}^{(0)}[7] \oplus A_{\text{DL}}^{(0)}[8] \oplus A_{\text{DL}}^{(0)}[10] \oplus A_{\text{DL}}^{(0)}[13] = \mathbf{c}[0] \\ A_{\text{DL}}^{(0)}[0] \oplus A_{\text{DL}}^{(0)}[4] \oplus A_{\text{DL}}^{(0)}[5] \oplus A_{\text{DL}}^{(0)}[9] \oplus A_{\text{DL}}^{(0)}[11] \oplus A_{\text{DL}}^{(0)}[14] = \mathbf{c}[1] \end{cases}$$

447 In the forward computation path, there are 11 constraints imposed on the ■
 448 cells. During the DL operation in the 2nd round, 6 constraints are imposed on
 449 the ■ cells. The specific expression of the constraints is shown in as follows:

$$\begin{cases} A_{\text{SL}}^{(1)}[4] \oplus A_{\text{SL}}^{(1)}[6] \oplus A_{\text{SL}}^{(1)}[8] \oplus A_{\text{SL}}^{(1)}[9] \oplus A_{\text{SL}}^{(1)}[13] \oplus A_{\text{SL}}^{(1)}[14] = \mathbf{c}[2] \\ A_{\text{SL}}^{(1)}[4] \oplus A_{\text{SL}}^{(1)}[9] \oplus A_{\text{SL}}^{(1)}[10] \oplus A_{\text{SL}}^{(1)}[14] \oplus A_{\text{SL}}^{(1)}[15] = \mathbf{c}[3] \\ A_{\text{SL}}^{(1)}[2] \oplus A_{\text{SL}}^{(1)}[5] \oplus A_{\text{SL}}^{(1)}[6] \oplus A_{\text{SL}}^{(1)}[8] \oplus A_{\text{SL}}^{(1)}[13] \oplus A_{\text{SL}}^{(1)}[15] = \mathbf{c}[4] \\ A_{\text{SL}}^{(1)}[0] \oplus A_{\text{SL}}^{(1)}[6] \oplus A_{\text{SL}}^{(1)}[7] \oplus A_{\text{SL}}^{(1)}[8] \oplus A_{\text{SL}}^{(1)}[10] \oplus A_{\text{SL}}^{(1)}[13] = \mathbf{c}[5] \\ A_{\text{SL}}^{(1)}[5] \oplus A_{\text{SL}}^{(1)}[7] \oplus A_{\text{SL}}^{(1)}[10] \oplus A_{\text{SL}}^{(1)}[11] = \mathbf{c}[6] \\ A_{\text{SL}}^{(1)}[10] \oplus A_{\text{SL}}^{(1)}[11] \oplus A_{\text{SL}}^{(1)}[12] \oplus A_{\text{SL}}^{(1)}[15] = \mathbf{c}[7] \end{cases}$$

450 Based on the above 6 constraints ($\mathbf{c}[2], \mathbf{c}[3], \mathbf{c}[4], \mathbf{c}[5], \mathbf{c}[6], \mathbf{c}[7]$), the effect of the ■
 451 cells on the 7 cells $A_{\text{DL}}^{(1)}[0, 5, 7, 10, 11, 13, 14]$ can be cancelled as follows:

$$\begin{cases} A_{\text{SL}}^{(1)}[4] \oplus A_{\text{SL}}^{(1)}[6] \oplus A_{\text{SL}}^{(1)}[8] \oplus A_{\text{SL}}^{(1)}[9] \oplus A_{\text{SL}}^{(1)}[13] \oplus A_{\text{SL}}^{(1)}[14] = \mathbf{c}[2] \\ A_{\text{SL}}^{(1)}[4] \oplus A_{\text{SL}}^{(1)}[9] \oplus A_{\text{SL}}^{(1)}[10] \oplus A_{\text{SL}}^{(1)}[14] \oplus A_{\text{SL}}^{(1)}[15] = \mathbf{c}[3] \\ A_{\text{SL}}^{(1)}[6] \oplus A_{\text{SL}}^{(1)}[8] \oplus A_{\text{SL}}^{(1)}[11] \oplus A_{\text{SL}}^{(1)}[12] \oplus A_{\text{SL}}^{(1)}[13] = \mathbf{c}[2] \oplus \mathbf{c}[3] \oplus \mathbf{c}[7] \\ A_{\text{SL}}^{(1)}[2] \oplus A_{\text{SL}}^{(1)}[5] \oplus A_{\text{SL}}^{(1)}[6] \oplus A_{\text{SL}}^{(1)}[8] \oplus A_{\text{SL}}^{(1)}[13] \oplus A_{\text{SL}}^{(1)}[15] = \mathbf{c}[4] \\ A_{\text{SL}}^{(1)}[2] \oplus A_{\text{SL}}^{(1)}[4] \oplus A_{\text{SL}}^{(1)}[7] \oplus A_{\text{SL}}^{(1)}[9] \oplus A_{\text{SL}}^{(1)}[12] \oplus A_{\text{SL}}^{(1)}[14] = \mathbf{c}[2] \oplus \mathbf{c}[4] \oplus \mathbf{c}[6] \oplus \mathbf{c}[7] \\ A_{\text{SL}}^{(1)}[0] \oplus A_{\text{SL}}^{(1)}[6] \oplus A_{\text{SL}}^{(1)}[7] \oplus A_{\text{SL}}^{(1)}[8] \oplus A_{\text{SL}}^{(1)}[10] \oplus A_{\text{SL}}^{(1)}[13] = \mathbf{c}[5] \\ A_{\text{SL}}^{(1)}[0] \oplus A_{\text{SL}}^{(1)}[4] \oplus A_{\text{SL}}^{(1)}[5] \oplus A_{\text{SL}}^{(1)}[9] \oplus A_{\text{SL}}^{(1)}[11] \oplus A_{\text{SL}}^{(1)}[14] = \mathbf{c}[2] \oplus \mathbf{c}[5] \oplus \mathbf{c}[6] \end{cases}$$

452 In a similar way, the 5 constraints ($\mathbf{c}[8], \mathbf{c}[9], \mathbf{c}[10], \mathbf{c}[11], \mathbf{c}[12]$) imposed on the \blacksquare
 453 cells through the DL in the 3rd round are enough to cancel the effect of the \blacksquare cells
 454 on the 6 cells $A_{\text{DL}}^{(2)}[4, 6, 8, 9, 13, 14]$. For the specific expression of the constraints,
 455 please refer to Algorithm 5 in Appendix C. And the detailed DoFs consumption
 456 process is illustrated as follows:

$$\begin{cases} A_{\text{SL}}^{(2)}[2] \oplus A_{\text{SL}}^{(2)}[8] \oplus A_{\text{SL}}^{(2)}[15] = \mathbf{c}[8] \\ A_{\text{SL}}^{(2)}[2] \oplus A_{\text{SL}}^{(2)}[9] \oplus A_{\text{SL}}^{(2)}[12] = \mathbf{c}[8] \oplus \mathbf{c}[12] \\ A_{\text{SL}}^{(2)}[1] \oplus A_{\text{SL}}^{(2)}[4] \oplus A_{\text{SL}}^{(2)}[15] = \mathbf{c}[9] \\ A_{\text{SL}}^{(2)}[1] \oplus A_{\text{SL}}^{(2)}[6] \oplus A_{\text{SL}}^{(2)}[12] = \mathbf{c}[9] \oplus \mathbf{c}[11] \\ A_{\text{SL}}^{(2)}[3] \oplus A_{\text{SL}}^{(2)}[6] \oplus A_{\text{SL}}^{(2)}[8] = \mathbf{c}[10] \\ A_{\text{SL}}^{(2)}[3] \oplus A_{\text{SL}}^{(2)}[4] \oplus A_{\text{SL}}^{(2)}[9] = \mathbf{c}[10] \oplus \mathbf{c}[11] \oplus \mathbf{c}[12] \end{cases}$$

457 In summary, the values of $l_{\mathcal{R}} = 13$ constraints can be determined for given values
 458 of $\lambda_{\mathcal{R}} = 14$ \blacksquare cells in $A^{(1)}$. Hence, we get $d_{\mathcal{B}} = 1$, $d_{\mathcal{R}} = \lambda_{\mathcal{R}} - l_{\mathcal{R}} = 1$.

459 *Matching process.* The matching points are $A_{\text{SL}}^{(4)}, A_{\text{DL}}^{(4)}$, indirect matching through
 460 the DL provides one-byte match, i.e., DoM = 1. The specific matching process is
 461 Equation (9).

$$A_{\text{SL}}^{(4)}[0] \oplus A_{\text{DL}}^{(4)}[13] \oplus A_{\text{DL}}^{(4)}[14] = A_{\text{DL}}^{(4)}[3] \oplus A_{\text{DL}}^{(4)}[4] \oplus A_{\text{DL}}^{(4)}[6] \oplus A_{\text{DL}}^{(4)}[8] \oplus A_{\text{DL}}^{(4)}[9] \quad (9)$$

462 Based on the above MitM framework, combined with the table-based tech-
 463 nique for solving nonlinear constrained neutral words [13], Algorithm 5 gives a
 464 detailed attack procedure in Appendix C.

465 *Complexity.* The nonlinear constraints imposed on \blacksquare cells are solved in Lines 2-8
 466 of Algorithm 5. That is, 14 \blacksquare cells of $A^{(1)}[0, 2, 4-15]$ are traversed to compute
 467 the exact values of $\mathbf{c}_{\mathcal{R}}[0-12]$. Then, the values of $A^{(1)}[0, 2, 4-15]$ are stored in a
 468 hash table V under the index of $\mathbf{c}_{\mathcal{R}}[0-12]$. Hence, the time complexity of the
 469 precomputation phase is $2^{8 \times 14} = 2^{112}$. The memory complexity is also 2^{112} to
 470 store table V .

471 Lines 10-24 of Algorithm 5 stand for one MitM episode. With the parameters
 472 $(d_{\mathcal{B}}, d_{\mathcal{R}}, d_m) = (1, 1, 1)$, there are a total of $2^{8 \times (1+1-1)} = 2^8$ solutions that can

be filtered out according to Equation (9). In order to find a full match of 128-bit, it's expected to repeat $2^{120-8} = 2^{112}$ MitM episodes. By traversing the \blacksquare in $A^{(1)}$ at the outer loop and enumerating the 13 constraints imposed on \blacksquare cells, it is sufficient to find a full match. According to Equation (1), The total time complexity of the attack phase is

$$2^8 \times 2^{112} + 2^{8 \times (16 - \min\{1,1,1\})} \approx 2^{120}.$$

The memory complexity is dominated by the table V of 2^{112} . And this attack can be converted to a preimage attack with a time complexity of 2^{125} according to [24, Fact9.99].

7 Conclusion

In this paper, we propose the **n-XOR** model to simulate the **XOR** operation with an arbitrary number of input cells. Specifically, the size of **n-XOR** model is independent of the number of input cells, and thus it is well suitable for primitives with a binary matrix as the diffusion layer. To eliminate the subtle inaccuracies caused by **n-XOR** model, we introduce another check model to determine the exact DoFs consumption of MitM attributes propagation. However, the size of the check model is still limited by the number of input cells n and does not work well when $n > 4$ in this paper. We expect that there will be more elegant and efficient techniques to overcome this defect and we leave this as an open problem.

We apply the above two new models to a MitM key recovery attack on 11-round **Midori64** with low data and memory. Besides, when omitting the whitening layers, two 12-round MitM characteristics for key recovery attack are found for optimizing time and data, respectively. For hash functions, we obtain improved preimage attack on 14-round weakened **Camellia-MM0** and 6-round **Aria-DM**. Both attacks are improved by 1 round compared to previous best records.

References

1. Aoki, K., Ichikawa, T., Kanda, M., Matsui, M., Moriai, S., Nakajima, J., Tokita, T.: Camellia: A 128-bit block cipher suitable for multiple platforms — design and analysis. In: Selected Areas in Cryptography. pp. 39–56. Springer Berlin Heidelberg (2001). https://doi.org/10.1007/3-540-44983-3_4
2. Aoki, K., Sasaki, Y.: Preimage attacks on one-block md4, 63-step md5 and more. In: Selected Areas in Cryptography. pp. 103–119. Springer Berlin Heidelberg (2009). https://doi.org/10.1007/978-3-642-04159-4_7
3. Aumasson, J., Meier, W., Mendel, F.: Preimage attacks on 3-pass HAVAL and step-reduced MD5. In: SAC. vol. 5381, pp. 120–135 (2008). https://doi.org/10.1007/978-3-642-04159-4_8
4. Baek, S., Kim, J.: Quantum rebound attacks on reduced-round ARIA-based hash functions. Cryptology ePrint Archive, Paper 2022/1604 (2022), <https://eprint.iacr.org/2022/1604>

- 511 5. Banik, S., Bogdanov, A., Isobe, T., Shibutani, K., Hiwatari, H., Akishita,
512 T., Regazzoni, F.: Midori: A block cipher for low energy. In: ASIACRYPT
513 2015. pp. 411–436. Springer Berlin Heidelberg (2015). [https://doi.org/10.1007/](https://doi.org/10.1007/978-3-662-48800-3_17)
514 [978-3-662-48800-3_17](https://doi.org/10.1007/978-3-662-48800-3_17)
- 515 6. Bao, Z., Dong, X., Guo, J., Li, Z., Shi, D., Sun, S., Wang, X.: Automatic search
516 of meet-in-the-middle preimage attacks on aes-like hashing. In: EUROCRYPT
517 2021. pp. 771–804. Springer International Publishing (2021). [https://doi.org/](https://doi.org/10.1007/978-3-030-77870-5_27)
518 [10.1007/978-3-030-77870-5_27](https://doi.org/10.1007/978-3-030-77870-5_27)
- 519 7. Bao, Z., Guo, J., Shi, D., Tu, Y.: Superposition meet-in-the-middle attacks:
520 updates on fundamental security of aes-like hashing. In: Annual International
521 Cryptology Conference. pp. 64–93. Springer (2022). [https://doi.org/10.1007/](https://doi.org/10.1007/978-3-031-15802-5_3)
522 [978-3-031-15802-5_3](https://doi.org/10.1007/978-3-031-15802-5_3)
- 523 8. Bogdanov, A., Khovratovich, D., Rechberger, C.: Biclique cryptanalysis of the full
524 aes. In: Advances in Cryptology – ASIACRYPT 2011. pp. 344–371. Springer Berlin
525 Heidelberg (2011). https://doi.org/10.1007/978-3-642-25385-0_19
- 526 9. Bogdanov, A., Rechberger, C.: A 3-subset meet-in-the-middle attack: Cryptanaly-
527 sis of the lightweight block cipher ktantan. In: SAC. pp. 229–240. Springer Berlin
528 Heidelberg (2011). https://doi.org/10.1007/978-3-642-19574-7_16
- 529 10. Chen, S., Guo, J., List, E., Shi, D., Zhang, T.: Diving deep into the preimage
530 security of aes-like hashing. Cryptology ePrint Archive, Paper 2024/300 (2024),
531 <https://eprint.iacr.org/2024/300>
- 532 11. Degré, M., Derbez, P., Lahaye, L., Schrottenloher, A.: New models for the crypt-
533 analysis of ascon. Cryptology ePrint Archive, Paper 2024/298 (2024), [https:](https://eprint.iacr.org/2024/298)
534 [//eprint.iacr.org/2024/298](https://eprint.iacr.org/2024/298)
- 535 12. Diffie, W., Hellman, M.E.: Special feature exhaustive cryptanalysis of the NBS
536 data encryption standard. Computer **10**(6), 74–84 (1977). [https://doi.org/10.](https://doi.org/10.1109/C-M.1977.217750)
537 [1109/C-M.1977.217750](https://doi.org/10.1109/C-M.1977.217750)
- 538 13. Dong, X., Hua, J., Sun, S., Li, Z., Wang, X., Hu, L.: Meet-in-the-middle attacks
539 revisited: Key-recovery, collision, and preimage attacks. In: CRYPTO 2021. pp.
540 278–308. Springer International Publishing (2021). [https://doi.org/10.1007/](https://doi.org/10.1007/978-3-030-84252-9_10)
541 [978-3-030-84252-9_10](https://doi.org/10.1007/978-3-030-84252-9_10)
- 542 14. Fuhr, T., Minaud, B.: Match box meet-in-the-middle attack against KATAN. In:
543 FSE 2014. pp. 61–81 (2014). https://doi.org/10.1007/978-3-662-46706-0_4
- 544 15. Gurobi Optimization, LLC: Gurobi Optimizer Reference Manual (2023), [https:](https://www.gurobi.com)
545 [//www.gurobi.com](https://www.gurobi.com)
- 546 16. Hong, D., Koo, B., Kim, D.C.: Preimage and second-preimage attacks on pgv
547 hashing modes of round-reduced aria, camellia, and serpent. IEICE T Fund Electr
548 **95**(1), 372–380 (2012), <https://api.semanticscholar.org/CorpusID:19830401>
- 549 17. Hou, Q., Dong, X., Qin, L., Zhang, G., Wang, X.: Automated meet-in-the-middle
550 attack goes to feistel. In: ASIACRYPT 2023. pp. 370–404. Springer Nature Singa-
551 pore (2023). https://doi.org/10.1007/978-981-99-8727-6_13
- 552 18. Isobe, T.: A single-key attack on the full gost block cipher. Journal of cryptology
553 **26**, 172–189 (2013). <https://doi.org/10.1007/s00145-012-9118-5>
- 554 19. ISO/IEC: 10118-2:2010 Information technology — Security techniques - Hash-
555 functions - Part 2: Hash-functions using an n-bit block cipher, 3rd edn (2010)
- 556 20. ISO/IEC 18033-3:2010 Information technology-Security techniques-
557 EncryptionAlgorithms-Part 3: Block ciphers (2010)
- 558 21. Kwon, D., Kim, J., Park, S., Sung, S.H., Sohn, Y., Song, J.H., Yeom, Y., Yoon,
559 E.J., Lee, S., Lee, J., et al.: New block cipher: Aria. In: Inscrypt. pp. 432–445.
560 Springer (2003). https://doi.org/10.1007/978-3-540-24691-6_32

- 561 22. Lin, L., Wu, W.: Meet-in-the-middle attacks on reduced-round midori64. IACR
562 ToSC pp. 215–239 (2017). <https://doi.org/10.13154/tosc.v2017.i1.215-239>
- 563 23. Liu, Y., Xiang, Z., Chen, S., Zhang, S., Zeng, X.: A novel automatic technique based
564 on milp to search for impossible differentials. In: ACNS. pp. 119–148. Springer
565 Nature Switzerland (2023). https://doi.org/10.1007/978-3-031-33488-7_5
- 566 24. Menezes, A.J., Vanstone, S.A., Oorschot, P.C.V.: Handbook of Applied Cryptog-
567 raphy. CRC Press, Inc., USA, 1st edn. (1996)
- 568 25. Preneel, B., Govaerts, R., Vandewalle, J.: Hash functions based on block ciphers:
569 a synthetic approach. In: Advances in Cryptology — CRYPTO’ 93. pp. 368–378.
570 Springer Berlin Heidelberg (1994). https://doi.org/10.1007/3-540-48329-2_31
- 571 26. Sasaki, Y.: Meet-in-the-middle preimage attacks on aes hashing modes and an
572 application to whirlpool. In: FSE. pp. 378–396. Springer Berlin Heidelberg (2011).
573 https://doi.org/10.1007/978-3-642-21702-9_22
- 574 27. Sasaki, Y.: Preimage attacks on feistel-sp functions: Impact of omitting the last
575 network twist. In: ACNS. pp. 170–185. Springer Berlin Heidelberg (2013). https://doi.org/10.1007/978-3-642-38980-1_11
- 576 28. Sasaki, Y.: Preimage attacks on feistel-sp functions: Impact of omitting the last
577 network twist. IEICE T Fund Electr **98**(1), 61–71 (2015). <https://doi.org/10.1587/transfun.E98.A.61>
- 578 29. Sasaki, Y.: Integer linear programming for three-subset meet-in-the-middle attacks:
579 Application to GIFT. In: IWSEC 2018. vol. 11049, pp. 227–243 (2018). https://doi.org/10.1007/978-3-319-97916-8_15
- 580 30. Sasaki, Y., Aoki, K.: Finding preimages in full MD5 faster than exhaustive search.
581 In: EUROCRYPT 2009, Proceedings. vol. 5479, pp. 134–152. Springer (2009).
582 https://doi.org/10.1007/978-3-642-01001-9_8
- 583 31. Sasaki, Y., Emami, S., Hong, D., Kumar, A.: Improved known-key distinguishers
584 on feistel-sp ciphers and application to camellia. In: Information Security and Pri-
585 vacy. pp. 87–100. Springer Berlin Heidelberg (2012). https://doi.org/10.1007/978-3-642-31448-3_7
- 586 32. Sasaki, Y., Wang, L., Sakai, Y., Sakiyama, K., Ohta, K.: Three-subset meet-in-the-
587 middle attack on reduced xtea. In: AFRICACRYPT 2012. pp. 138–154. Springer
588 Berlin Heidelberg (2012). https://doi.org/10.1007/978-3-642-31410-0_9
- 589 33. Schrottenloher, A., Stevens, M.: Simplified mitm modeling for permutations: New
590 (quantum) attacks. In: CRYPTO 2022. pp. 717–747. Springer Nature Switzerland
591 (2022). https://doi.org/10.1007/978-3-031-15982-4_24
- 592 34. Schrottenloher, A., Stevens, M.: Simplified modeling of mitm attacks for block
593 ciphers: New (quantum) attacks. IACR Transactions on Symmetric Cryptology
594 **2023**, 146–183 (2023). <https://doi.org/10.46586/tosc.v2023.i3.146-183>
- 595 35. Shahmirzadi, A.R., Azimi, S.A., Salmasizadeh, M., Mohajeri, J., Aref, M.R.: Im-
596 possible differential cryptanalysis of reduced-round midori64 block cipher. In: IS-
597 CISC. pp. 99–104 (Sep 2017). <https://doi.org/10.1109/ISCISC.2017.8488362>
- 598 36. Sun, S., Hu, L., Wang, P., Qiao, K., Ma, X., Song, L.: Automatic security evalu-
599 ation and (related-key) differential characteristic search: Application to SIMON,
600 PRESENT, LBlock, DES(L) and other bit-oriented block ciphers. In: ASIACRYPT
601 2014. pp. 158–178 (2014). https://doi.org/10.1007/978-3-662-45611-8_9
- 602 37. Wei, L., Rechberger, C., Guo, J., Wu, H., Wang, H., Ling, S.: Improved meet-
603 in-the-middle cryptanalysis of ktantan (poster). In: Information Security and Pri-
604 vacy. pp. 433–438. Springer Berlin Heidelberg (2011). https://doi.org/10.1007/978-3-642-22497-3_31
- 605
- 606
- 607
- 608
- 609

610 A Details of MILP Models for MitM Attack

611 In this section, we briefly recall the MILP model for MC and XOR operation of
612 AES in [6].

613 **The MC.** The rules of the MC are formalized in two different directions in
614 [6]. Taking the forward computation as an example, the set of rules is given as
615 follows:

- 616 1. If there is at least one \square in the input column, all the outputs are \square ;
- 617 2. If there are \blacksquare but no \square and $\color{red}\blacksquare$ in the input column, then all the outputs are
618 \blacksquare ;
- 619 3. If all the inputs are \blacksquare , then all the outputs are \blacksquare ;
- 620 4. If there are $\color{red}\blacksquare$ and \blacksquare but no \square in the input column, each output must be \blacksquare
621 or \square . Moreover, the sum of the numbers of \blacksquare and \blacksquare in the input and output
622 columns must be no more than 3;
- 623 5. If there are $\color{red}\blacksquare$ but no \square and \blacksquare in the input column, then each output must
624 be $\color{red}\blacksquare$ or \blacksquare . Moreover, the number of \blacksquare in the input and output columns must
625 be no more than 3.

626 Some examples of valid coloring schemes of the MC-RULE in the forward compu-
627 tation are shown in Figure 12.

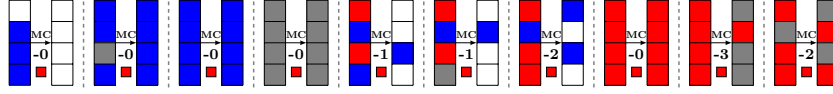


Fig. 12: Some valid coloring schemes for MC in forward computation in [6]

628 Let $(\alpha[0], \alpha[1], \alpha[2], \alpha[3])^T$ and $(\beta[0], \beta[1], \beta[2], \beta[3])^T$ be the input and output
629 columns. In [6], Bao *et al.* use three 0-1 indicator variables μ, v, ω for the input
630 column to fulfill different rules auxiliary. Let $\mu = 1$ if and only if there exists
631 $i \in \{0, 1, 2, 3\}$ such that $(x_i^\alpha, y_i^\alpha) = (0, 0)$. Let $v = 1$ if and only if $x_i^\alpha = 1$ for
632 each $i \in \{0, 1, 2, 3\}$. Let $\omega = 1$ if and only if $y_i^\alpha = 1$ for each $i \in \{0, 1, 2, 3\}$.
633 Then, with the help of μ, v, ω , the MC-RULE in the forward computation can be
634 described as a system of inequalities:

$$\left\{ \begin{array}{l} \sum_{i=0}^3 x_i^\alpha - 4v \geq 0; \\ \sum_{i=0}^3 x_i^\alpha - v \leq 3. \end{array} \right. \left| \begin{array}{l} \sum_{i=0}^3 x_i^\beta + 4\mu \leq 4; \\ \sum_{i=0}^3 y_i^\beta + 4\mu \leq 4; \\ \sum_{i=0}^3 y_i^\beta - 4\omega = 0; \end{array} \right. \left\{ \begin{array}{l} \sum_{i=0}^3 (x_i^\alpha + x_i^\beta) - 5v \leq 3; \\ \sum_{i=0}^3 (x_i^\alpha + x_i^\beta) - 8v \geq 0. \end{array} \right.$$

635 **The XOR.** For the XOR operation in two different directions, the coloring
 636 schemes of the input and output cells are shown in Figure 13.

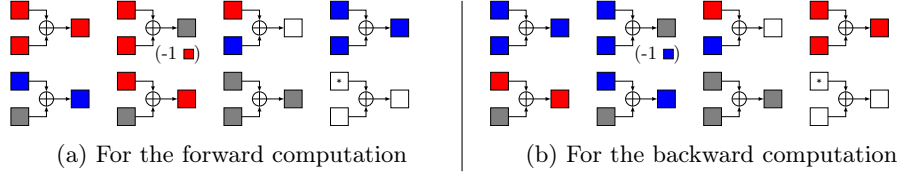


Fig. 13: The XOR in [6], where a “*” means that the cell can be any color

636 Let $\alpha[i]$, $\beta[i]$ denote the input cells and $\gamma[i]$ denote the output cell, where
 637 $0 \leq i \leq 15$. Let a boolean variable d_i indicate the consumption of DoF, where
 638 $d_i = 1$ means that one DoF is consumed to let the corresponding output be \blacksquare .
 639 The set of rules restrict $(x_i^\alpha, y_i^\alpha, x_i^\beta, y_i^\beta, x_i^\gamma, y_i^\gamma, d_i)$ to a subset of \mathbb{F}_2^7 , which can
 640 be described by a system of linear inequalities with the convex hull technique in
 641 [36].
 642

643 B Descriptions of Midori, Camellia and Aria

644 B.1 Specification of Midori

645 Midori is a family of SPN-based lightweight block cipher designed by Banik *et*
 646 *al.* at ASIACRYPT 2015 [5]. Two versions of Midori use a 64-bit and a 128-bit
 647 internal state, respectively. In this work, we focus on the 64-bit version denoted
 648 by Midori64. The internal state of Midori64 can be represented as a 4×4 array
 649 as shown in Figure 14. Midori64 is of 16 iterated rounds and each round function
 650 consists of four operations:

- 651 - **SubCell** (SC): Apply the 4-bit non-linear involution S-box on each nibble.
- 652 - **ShuffleCell** (ShC): Update the position of each nibble by a pre-defined
 653 permutation.
- 654 - **MixColumn** (MC): Each column is left multiplied by a 4×4 binary matrix
 655 M as follows.

$$M = \begin{pmatrix} 0 & 1 & 1 & 1 \\ 1 & 0 & 1 & 1 \\ 1 & 1 & 0 & 1 \\ 1 & 1 & 1 & 0 \end{pmatrix}.$$

- 656 - **KeyAdd** (KA): A round key is XORed to the internal state.

657 For the last round, the operations ShC, MC and KA are omitted. Two sub-keys
 658 $K^{(0)} \| K^{(1)}$ are derived from the 128-bit master key K and the round keys are
 659 generated by $K^{(r \% 2)} \oplus \alpha_r$ alternatively, where $0 \leq r \leq 14$ and α_r is a round
 660 constant. Besides, additional KA operations are applied with a whitening key
 661 $WK = K^{(0)} \oplus K^{(1)}$ before the first round and after the last round.

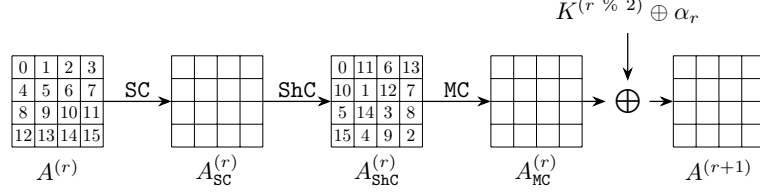


Fig. 14: One full round function of Midori64

B.2 Specification of Camellia

Camellia is a Feistel-based block cipher designed by NTT and Mitsubishi Electric Corporation [1] and has been specified in ISO/IEC 18033-3:2010 [20]. This work only targets on the weakened version of Camellia with 128 bits block and key size, where the FL/FL^{-1} transformations and whitening layers are omitted. The iterated round function consists of AddRoundKey (AK), SubBytes (SB) and MixColumns (MC) as shown in Figure 15. The linear layer of MC is a 8×8 binary matrix described as follows.

$$P = \begin{pmatrix} 1 & 0 & 1 & 1 & 0 & 1 & 1 & 1 \\ 1 & 1 & 0 & 1 & 1 & 0 & 1 & 1 \\ 1 & 1 & 1 & 0 & 1 & 1 & 0 & 1 \\ 0 & 1 & 1 & 1 & 1 & 1 & 1 & 0 \\ 1 & 1 & 0 & 0 & 0 & 1 & 1 & 1 \\ 0 & 1 & 1 & 0 & 1 & 0 & 1 & 1 \\ 0 & 0 & 1 & 1 & 1 & 1 & 0 & 1 \\ 1 & 0 & 0 & 1 & 1 & 1 & 1 & 0 \end{pmatrix}.$$

The key schedule takes a 128-bit key $K = K' \| K''$ as the input of 4-round Feistel structure, as shown in Figure 15, to compute another 128-bit key $K_A = K'_A \| K''_A$. The round function is borrowed from the encryption, where the round keys are pre-defined constants. Then, each round key k_i can be derived from the rotation of K or K_A . Since we only focus on $(k_0, k_1, k_{12}, k_{13})$, we omit detailed key schedule here.

B.3 Specification of Aria

Aria was proposed by Korean researchers at ICISC 2003 [21] and the version 1.2 was subsequently included in the Korean Standard (KS X1213) in 2004. In this paper, we focus our attention on Aria-128, which refers to both the block and key sizes are 128 bits, and which we henceforth abbreviate as Aria. Aria is based on SPN structure with 12 rounds, and each round except the last one consists of Substitution-Layer (SL), Diffusion-Layer (DL) and AddRoundKey (AK) as shown in Figure 16. In the last round, the DL is omitted. Before the first round, a whitening key is XORed to the plaintext. The updated matrix P used in

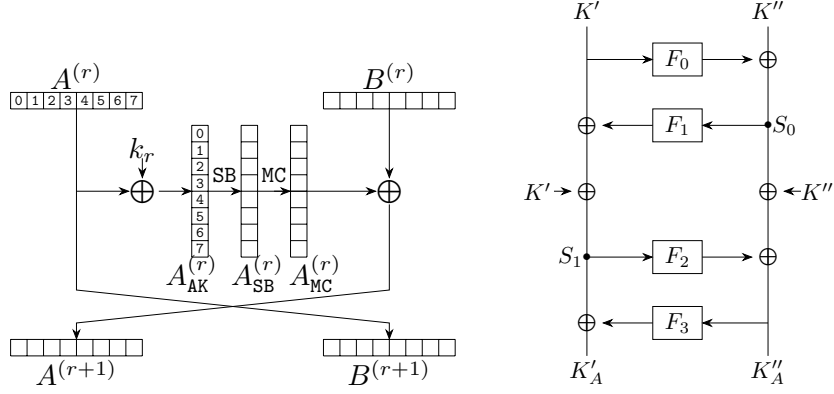


Fig. 15: One full round function of **Camellia** and the key schedule of **Camellia**

DL is a 16×16 binary matrix described as follows.

$$P = \begin{pmatrix} 0 & 0 & 0 & 1 & 1 & 0 & 1 & 0 & 1 & 1 & 1 & 0 & 0 & 0 & 1 & 1 & 0 \\ 0 & 0 & 1 & 0 & 0 & 1 & 0 & 1 & 1 & 1 & 1 & 0 & 0 & 1 & 0 & 0 & 1 \\ 0 & 1 & 0 & 0 & 1 & 0 & 1 & 0 & 0 & 0 & 1 & 1 & 1 & 0 & 0 & 1 & 0 \\ 1 & 0 & 0 & 0 & 0 & 1 & 0 & 1 & 0 & 0 & 1 & 1 & 0 & 1 & 1 & 0 & 0 \\ 1 & 0 & 1 & 0 & 0 & 1 & 0 & 0 & 1 & 0 & 0 & 1 & 0 & 0 & 1 & 1 & 0 \\ 0 & 1 & 0 & 1 & 1 & 0 & 0 & 0 & 0 & 1 & 1 & 0 & 0 & 0 & 1 & 1 & 0 \\ 1 & 0 & 1 & 0 & 0 & 0 & 0 & 1 & 0 & 1 & 1 & 0 & 1 & 1 & 0 & 0 & 0 \\ 0 & 1 & 0 & 1 & 0 & 0 & 1 & 0 & 1 & 0 & 0 & 1 & 1 & 1 & 0 & 0 & 0 \\ 1 & 1 & 0 & 0 & 1 & 0 & 0 & 1 & 0 & 0 & 1 & 0 & 0 & 1 & 0 & 1 & 0 \\ 1 & 1 & 0 & 0 & 0 & 1 & 1 & 0 & 0 & 0 & 0 & 1 & 1 & 0 & 1 & 0 & 0 \\ 0 & 0 & 1 & 1 & 0 & 1 & 1 & 0 & 1 & 0 & 0 & 0 & 0 & 1 & 0 & 1 & 0 \\ 0 & 0 & 1 & 1 & 1 & 0 & 0 & 1 & 0 & 1 & 0 & 0 & 1 & 0 & 1 & 0 & 0 \\ 0 & 1 & 1 & 0 & 0 & 0 & 1 & 1 & 0 & 1 & 0 & 1 & 1 & 0 & 0 & 0 & 0 \\ 1 & 0 & 0 & 1 & 0 & 0 & 1 & 1 & 1 & 0 & 1 & 0 & 0 & 1 & 0 & 0 & 0 \\ 1 & 0 & 0 & 1 & 1 & 1 & 0 & 0 & 0 & 1 & 0 & 1 & 0 & 0 & 1 & 0 & 0 \\ 0 & 1 & 1 & 0 & 1 & 1 & 0 & 0 & 1 & 0 & 1 & 0 & 0 & 0 & 0 & 1 & 0 \end{pmatrix}.$$

In this paper, we target on the preimage attack on **Aria-DM**. Since the key is usually fixed as a constant in the DM hashing mode, we omit the description of the key schedule here.

C Figure and algorithms for Midori64 and Aria

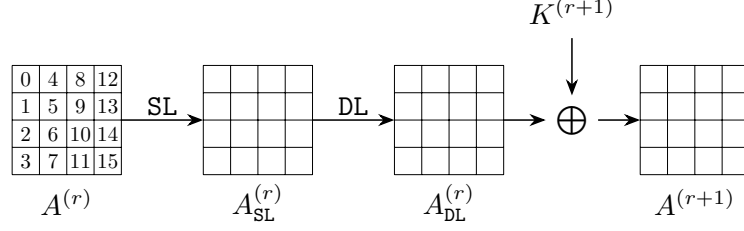


Fig. 16: One full round function of **Aria**

Algorithm 4: MitM Key Recovery Attack on 12-round weakened Midori64, , optimized for data complexity

```

1   $C[1, 3, 5, 8, 9, 13, 14] \leftarrow 0, A_{MC}^{(9)}[5, 9, 13] \leftarrow 0$ 
2   $A_{MC}^{(10)}[0] \oplus A_{MC}^{(10)}[4] \leftarrow 0, A_{MC}^{(10)}[0] \oplus A_{MC}^{(10)}[12] \leftarrow 0, A_{MC}^{(10)}[2] \oplus A_{MC}^{(10)}[6] \leftarrow 0,$ 
    $A_{MC}^{(10)}[2] \oplus A_{MC}^{(10)}[10] \leftarrow 0, A_{MC}^{(10)}[7] \oplus A_{MC}^{(10)}[11] \leftarrow 0, A_{MC}^{(10)}[7] \oplus A_{MC}^{(10)}[15] \leftarrow 0$ 
3  Collecting plaintext-ciphertext pairs by traversing the non-constant  $16 - 7 = 9$ 
   cells in  $C$ , and storing them in table  $H$ 
4  for all possible values of the  $\blacksquare$  cells in  $K^{(0)}$  and  $K^{(1)}$  do
5      for  $(c_{R,1}, c_{R,2}) \in \mathbb{F}_2^{2 \times 4}$  do
6          Derive the solution space  $\mathcal{S}_R$  of  $\blacksquare$  cells by
              
$$\begin{cases} K^{(0)}[5] \oplus K^{(0)}[9] = c_{R,1} \\ K^{(0)}[5] \oplus K^{(0)}[13] = c_{R,2} \end{cases}$$

7           $L \leftarrow []$ 
8          for  $v_R \in \mathcal{S}_R$  do
9              Compute  $A_{Shc}^{(4)}[0, 4]$  along the forward computation path:
10              $A_{MC}^{(9)} \rightarrow C \rightarrow Dec_K(C) \rightarrow A_{Shc}^{(4)}$  by accessing  $H$ 
11              $L[A_{Shc}^{(4)}[0] \oplus A_{Shc}^{(4)}[4]] \leftarrow v_R$ 
12         end
13         for  $2^4$  possible values of  $K^{(1)}[15]$  do
14             Compute  $A_{MC}^{(4)}[0, 4]$  along the backward computation path:
15              $C \rightarrow A_{MC}^{(4)}$ 
16             for Candidate keys in  $L[A_{MC}^{(4)}[0] \oplus A_{MC}^{(4)}[4]]$  do
17                 Test the guessed key with several plaintext-ciphertext pairs
18             end
19         end
20 end
```

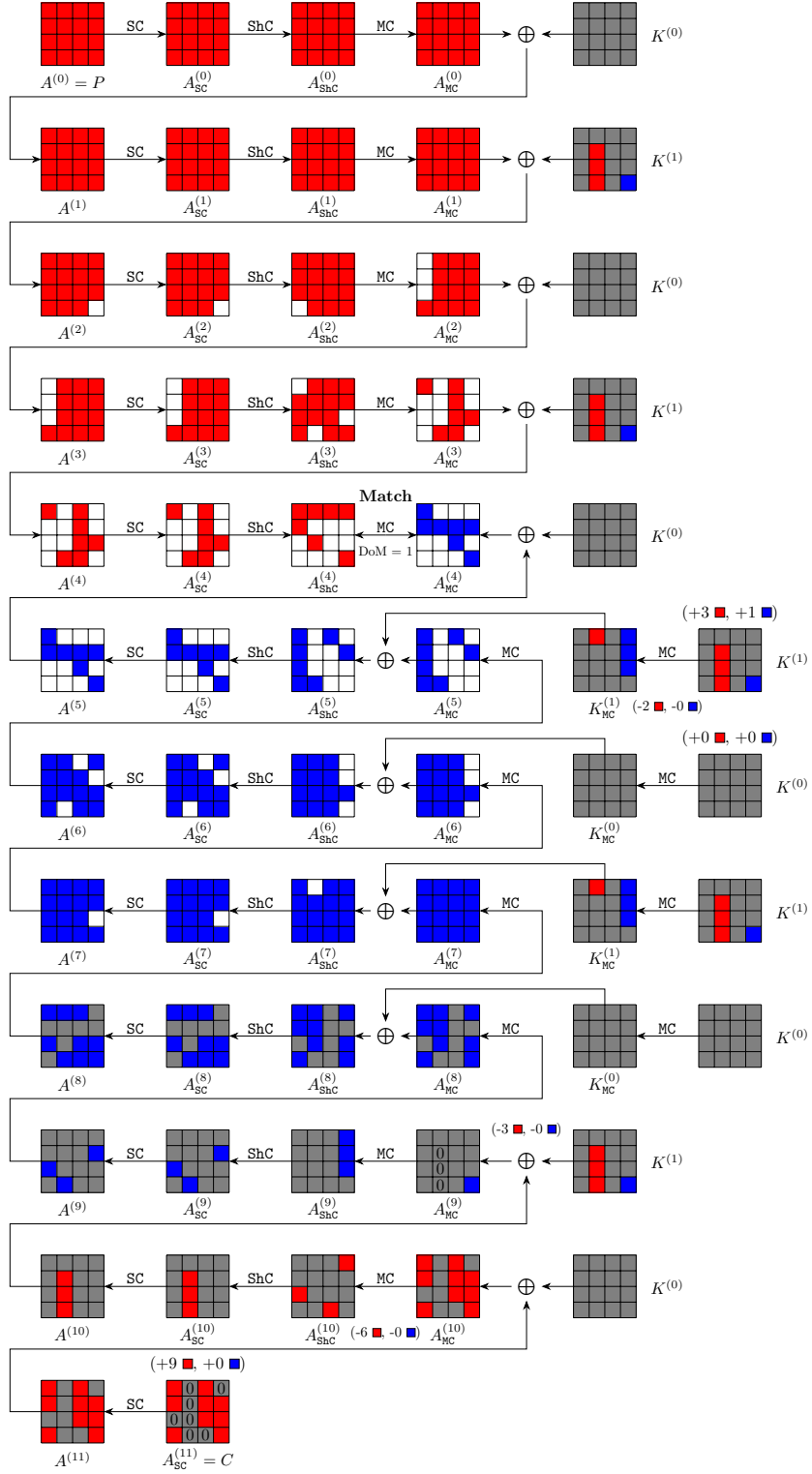


Fig.17: Meet-in-the-Middle key recovery attack on 12-round weakened Midori64, optimized for data complexity

Algorithm 5: MitM Pseudo-Preimage Attack on 6-round Aria-DM

```

1 for  $2^x$  possible values of  $\blacksquare$  in  $A^{(1)}$  /*  $x + 104 = 120 - 8$ , i.e.,  $x = 8$  */
2 do
3    $V \leftarrow []$ ;
4   for  $v_{\mathcal{R}} \in \mathbb{F}_2^{8 \times 14}$  in  $A^{(1)}$  do
5     Compute backward to get the values of the  $\blacksquare$  cells in  $A_{\text{DL}}^{(0)}$ ,
        
$$\begin{aligned} c_{\mathcal{R}}[0] &\leftarrow A_{\text{DL}}^{(0)}[0] \oplus A_{\text{DL}}^{(0)}[6] \oplus A_{\text{DL}}^{(0)}[7] \oplus A_{\text{DL}}^{(0)}[8] \oplus A_{\text{DL}}^{(0)}[10] \oplus A_{\text{DL}}^{(0)}[13], \\ c_{\mathcal{R}}[1] &\leftarrow A_{\text{DL}}^{(0)}[0] \oplus A_{\text{DL}}^{(0)}[4] \oplus A_{\text{DL}}^{(0)}[5] \oplus A_{\text{DL}}^{(0)}[9] \oplus A_{\text{DL}}^{(0)}[11] \oplus A_{\text{DL}}^{(0)}[14]. \end{aligned}$$

6     Compute forward to the  $\blacksquare$  cells in  $A_{\text{SL}}^{(1)}$  and  $A_{\text{SL}}^{(2)}$ ,
        
$$\begin{aligned} c_{\mathcal{R}}[2] &\leftarrow A_{\text{SL}}^{(1)}[4] \oplus A_{\text{SL}}^{(1)}[6] \oplus A_{\text{SL}}^{(1)}[8] \oplus A_{\text{SL}}^{(1)}[9] \oplus A_{\text{SL}}^{(1)}[13] \oplus A_{\text{SL}}^{(1)}[14], \\ c_{\mathcal{R}}[3] &\leftarrow A_{\text{SL}}^{(1)}[4] \oplus A_{\text{SL}}^{(1)}[9] \oplus A_{\text{SL}}^{(1)}[10] \oplus A_{\text{SL}}^{(1)}[14] \oplus A_{\text{SL}}^{(1)}[15], \\ c_{\mathcal{R}}[4] &\leftarrow A_{\text{SL}}^{(1)}[2] \oplus A_{\text{SL}}^{(1)}[5] \oplus A_{\text{SL}}^{(1)}[6] \oplus A_{\text{SL}}^{(1)}[8] \oplus A_{\text{SL}}^{(1)}[13] \oplus A_{\text{SL}}^{(1)}[15], \\ c_{\mathcal{R}}[5] &\leftarrow A_{\text{SL}}^{(1)}[0] \oplus A_{\text{SL}}^{(1)}[6] \oplus A_{\text{SL}}^{(1)}[7] \oplus A_{\text{SL}}^{(1)}[8] \oplus A_{\text{SL}}^{(1)}[10] \oplus A_{\text{SL}}^{(1)}[13], \\ c_{\mathcal{R}}[6] &\leftarrow A_{\text{SL}}^{(1)}[5] \oplus A_{\text{SL}}^{(1)}[7] \oplus A_{\text{SL}}^{(1)}[10] \oplus A_{\text{SL}}^{(1)}[11], \\ c_{\mathcal{R}}[7] &\leftarrow A_{\text{SL}}^{(1)}[10] \oplus A_{\text{SL}}^{(1)}[11] \oplus A_{\text{SL}}^{(1)}[12] \oplus A_{\text{SL}}^{(1)}[15], \\ c_{\mathcal{R}}[8] &\leftarrow A_{\text{SL}}^{(2)}[2] \oplus A_{\text{SL}}^{(2)}[8] \oplus A_{\text{SL}}^{(2)}[15], \\ c_{\mathcal{R}}[9] &\leftarrow A_{\text{SL}}^{(2)}[1] \oplus A_{\text{SL}}^{(2)}[4] \oplus A_{\text{SL}}^{(2)}[15], \\ c_{\mathcal{R}}[10] &\leftarrow A_{\text{SL}}^{(2)}[3] \oplus A_{\text{SL}}^{(2)}[6] \oplus A_{\text{SL}}^{(2)}[8], \\ c_{\mathcal{R}}[11] &\leftarrow A_{\text{SL}}^{(2)}[4] \oplus A_{\text{SL}}^{(2)}[6] \oplus A_{\text{SL}}^{(2)}[12] \oplus A_{\text{SL}}^{(2)}[15], \\ c_{\mathcal{R}}[12] &\leftarrow A_{\text{SL}}^{(2)}[8] \oplus A_{\text{SL}}^{(2)}[9] \oplus A_{\text{SL}}^{(2)}[12] \oplus A_{\text{SL}}^{(2)}[15]. \end{aligned}$$

7      $V[c_{\mathcal{R}}] \leftarrow v_{\mathcal{R}}$ ; /* There are  $2^8$  elements in  $V[c_{\mathcal{R}}]$  for each  $c_{\mathcal{R}}$  */
8   end
9   for  $c_{\mathcal{R}} \in \mathbb{F}_2^{8 \times 13}$  do
10     $L \leftarrow []$ 
11    for  $v_{\mathcal{R}} \in V[c_{\mathcal{R}}]$  do
12      Compute to the  $\blacksquare$  cells in  $A_{\text{DL}}^{(4)}$ , and one-byte  $End_{\mathcal{R}}$  for matching is
        derived by
13      
$$End_{\mathcal{R}} \leftarrow (A_{\text{DL}}^{(4)}[3] \oplus A_{\text{DL}}^{(4)}[4] \oplus A_{\text{DL}}^{(4)}[6] \oplus A_{\text{DL}}^{(4)}[8] \oplus A_{\text{DL}}^{(4)}[9])$$

14       $L[End_{\mathcal{R}}] \leftarrow v_{\mathcal{R}}$ 
15    end
16    for  $2^8$  possible values of  $A^{(1)}[3]$  do
17      Compute to the  $\blacksquare$  cells in  $A_{\text{DL}}^{(4)}$  and  $A_{\text{SL}}^{(4)}$ , derive one-byte  $End_{\mathcal{B}}$  for
        matching by
18      
$$End_{\mathcal{B}} \leftarrow (A_{\text{SL}}^{(4)}[0] \oplus A_{\text{DL}}^{(4)}[13] \oplus A_{\text{DL}}^{(4)}[14])$$

19      for  $v_{\mathcal{R}} \in L[End_{\mathcal{B}}]$  do
20        Reconstruct the (candidate) message  $X$ 
21        if  $X$  is a preimage then
22          Output  $X$  and stop
23        end
24      end
25    end
26  end
27 end
```
